Hybrid Control Strategy for the Autonomous Transition Flight of a Fixed-Wing Aircraft

Pedro Casau, David Cabecinhas, and Carlos Silvestre, *Member, IEEE*

Abstract—This paper develops a hybrid control strategy that provides autonomous transition between hovered and leveled flights to a model-scale fixed-wing aircraft. The aircraft's closed-loop dynamics are described by means of a hybrid automaton with the hover, transition, level, and recovery operating modes, each one corresponding to a different region of the flight envelope. Linear parameter varying control techniques are employed in hover and level, providing robust local stabilization, and a nonlinear locally input-to-state stable controller provides practical reference tracking to the transition operating mode. These controllers, together with an appropriate choice of reference maneuvers, ensure that a transition from hovered flight to level flight, or vice versa, is achieved. Whenever the aircraft state reaches unexpected values, the recovery controller is triggered in order to drive the aircraft toward stable hovered flight, providing a chance to retry the transition maneuver. The controllers' performance and robustness is assessed within a realistic simulation environment in the presence of sensor noise.

Index Terms—Aerospace applications, hybrid automata, nonlinear control, unmanned air vehicles (UAVs), vertical take-off and landing (VTOL) vehicles.

I. INTRODUCTION

OVER the last decade, the advent of new sensor technology and the success of already deployed platforms have bolstered a worldwide interest in developing and expanding the capabilities of uninhabited air vehicles (UAVs). These aerial vehicles provide unprecedented autonomy and efficiency when compared with standard aircrafts, built under the constraints imposed by the presence of a human pilot. An UAV bypasses many human limitations enabling several new features [1], such as high altitude operation, high endurance, reduced weight, more efficient structural and aerodynamic aircraft

designs, etc. New sights emerge in the fields of aircraft design and mission planning with the implementation of these features, giving birth to new application scenarios [2].

A particular application of interest is ocean surface data gathering. This application is still limited to a few scientific institutions scattered worldwide, and most vehicles have been designed to conduct simple survey missions that, in general, do not require close interaction between the operator and the environment. The effective use of UAVs in demanding marine science applications must be clearly demonstrated, namely by evaluating the system in terms of adaptability to different missions scenarios, maritime launch and recovery, survivability, autonomy, endurance, payload performance and usability, and system integration with the existing marine science instrumentation. Several UAV configurations, such as rotorcraft, ducted-fan vehicles, tilted-wing and fixed-wing aircraft, are being exploited in order to successfully meet these stringent requirements (see [3]–[7]). Each of these vehicles must be able to safely land and take-off on the deck of an available ship. Other applications include search and rescue in hazardous environments [8], fire mitigation [9], traffic monitoring [10], and targeting [1].

Fixed-wing aircraft with vertical take-off and landing (VTOL) capabilities are able to maneuver within exiguous environments while in hovered flight, and have a wide mission radius while in leveled flight, thus combining standard helicopter and airplane characteristics [11]. They provide superior endurance and comparable maneuverability to that of the rotorcraft UAVs, making them a preferable choice for the discussed application. In general, the vertical take-off and landing procedure for an autonomous air vehicle spans the regions of the flight envelope highlighted in Fig. 1. For a fixed-wing aircraft perched on a post, the standard take-off maneuver begins with the aircraft landed nose up, entering the hover flight region of the flight envelope when the thrust overcomes the weight, thus becoming airborne. The take-off sequence is then finalized by performing a pitch down maneuver, accompanied by a forward velocity increase, thereby achieving the transition from hover to level flight.

Several control strategies have been proposed in order to accomplish autonomous transition, including open-loop maneuvers [12], linear optimal techniques [13], locally stable nonlinear controllers [6], and adaptive controllers [14]. The work reported in [13] presents a nonlinear model which is used to produce full state feedback laws that locally stabilize the aircraft in both hover and level flight regions of the flight envelope. Open-loop maneuvers and switching between the two control laws enable autonomous take-off and landing within an indoors experimental setup. However, the open-loop
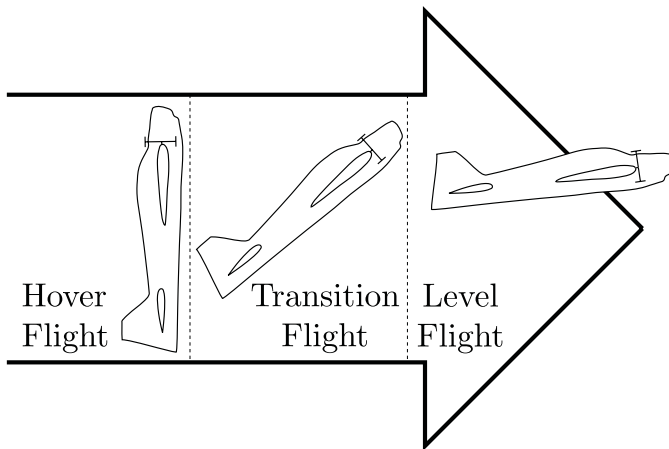
Fig. 1. Regions of the flight envelope spanned by a VTOL aircraft.

maneuvers and the switching logic are formulated specifically for the experimental setup at hand, and there is the lack of a systematic approach to the transition flight problem. The work developed in [6] addresses the transition problem much more carefully, presenting a formal definition of the hover and level flight regions of the flight envelope. Instead of linear controllers, as in [13], two nonlinear controllers perform path-following, providing robustness to the system as long as the reference trajectory remains far from the envelope boundaries. Switching is performed at the intersection between the two flight regions. This strategy is more systematic but it relies on aerodynamic force approximations for each flight region and, moreover, the pitch angle is directly considered as a control input which is obviously not the case for a real system.

This paper draws inspiration from these works and presents a solution for the autonomous transition flight problem, which resorts to the hybrid automata framework [15]. This framework allows for a complex model to be described in a modular way by collecting simpler dynamic models, each one describing an operating mode of the system. For the particular problem at hand, the operating modes correspond to the hover, transition and level flight regions of the flight envelope. Stabilization during hovered and leveled flight is achieved by means of linear optimal control techniques. We perform a model simplification in order to obtain a polytopic linear parameter varying (LPV) structure for the system, and the controllers for each flight regime are obtained as the solution to a linear matrix inequality optimization problem. This strategy provides local stabilizing controllers for trimming trajectories in a polytopic region of the state space [16]. The transition operating mode employs a nonlinear controller, which enables practical reference tracking. In order to enhance the system's robustness, a fourth operating mode is added to the automata providing "recovery" maneuvers whenever the aircraft faces overwhelming perturbations. A nonlinear controller that renders the hover equilibrium point globally asymptotically stable is used during this operating mode that is triggered if the aircraft state reaches out to unexpected values.

A preliminary version of this paper focused only on the design of a transition controller for a fixed-wing aircraft [17].

The present work also builds upon another work, which focused on the design of a recovery controller [18]. In this paper, we combine the controllers designed in [17] and [18] into a new hybrid automaton which guarantees that either: 1) the aircraft successfully performs the transition maneuver if the perturbations are confined within certain bounds or 2) it recovers to stable hovered flight if not.

The rest of this paper is organized as follows. Section II presents some notational conventions which are employed throughout this paper. Section III describes the aircraft model. The hybrid automaton and the robust maneuvers are defined in Sections IV and V. The controller design is presented in Section VI. Finally, some simulation results for the proposed control law are shown in Section VII, and concluding remarks are presented in Section VIII.

II. NOTATION

The set of rules that embody the mathematical equations throughout this text is presented in this section for improved clarity.

1) Scalar values are represented by either uppercase or lowercase letters (example: ρ and A).
2) Vectors are represented by boldface lowercase letters (example: $\mathbf{v}$).
3) Matrices are represented by boldface uppercase letters (example: $\mathbf{I}$).
4) Coordinate frames are represented by a capital letter in closed brackets (example: $\{I\}$).
5) The superscript $^{I}\mathbf{x}$ means that the vector $\mathbf{x}$ is written in the reference frame $\{I\}$.
6) The function $\text{atan2}(y, x)$ returns the angle $\gamma \in (-\pi, \pi]$ between point with coordinates (x, y) and the positive x-axis.
7) The operator $B_\epsilon(\mathbf{p})$ denotes a ball of radius ϵ around the point $\mathbf{p}$, i.e., the set of points $\mathbf{x}$ such that $\|\mathbf{x} - \mathbf{p}\| < \epsilon$.
8) The mapping denoted by co(.) is the convex hull operator.
9) The abbreviation w.r.t. stands for with respect to.
10) The definition of input-to-state stable (ISS) with restrictions for a dynamic system is taken from [19] and reproduced here for completeness. Consider the nonlinear system

$$\dot{x} = f(x, u) \qquad (1)$$

with state $x \in \mathbb{R}^n$, input $u \in \mathbb{R}^m$, in which $f(0, 0) = 0$ and $f(x, u)$ is locally Lipschitz on $\mathbb{R}^n \times \mathbb{R}^m$. Let X be an open subset of $\mathbb{R}^n$ containing the origin and let U be a positive number. System (1) is said to be input-to-state stable with restriction X on $x(0)$ and restriction U on $u(\cdot)$ if there exist class $\mathcal{K}$ functions $\gamma_0(\cdot)$ and $\gamma_u(\cdot)$ such that, for any $x(0) \in X$ and any input $u(\cdot) \in L_\infty^m$ satisfying $\|u(\cdot)\|_\infty < U$, the response $x(t)$ satisfies

$$\|x(\cdot)\|_\infty \le \max\{\gamma_0(\|x(0)\|), \gamma_u(\|u(\cdot)\|_\infty)\}$$
$$\limsup_{t \to \infty} \|x(t)\| \le \gamma_u(\limsup_{t \to \infty} \|u(t)\|).$$

11) A saturation function is a twice differentiable nondecreasing function $\sigma : \mathbb{R} \to \mathbb{R}$, which satisfies the following properties:

Fig. 2.   Model-scale aircraft in hovered flight.

a) $\sigma(0) = 0$;
b) $s\sigma(s) > 0$ for all $s \neq 0$;
c) $\lim_{s \to \pm\infty} \sigma(s) = \pm 1$.

12) The sign(.) function is given by

$$\text{sign}(x) = \begin{cases} 1, & \text{if } x > 0 \\ 0, & \text{if } x = 0 \\ -1, & \text{if } x < 0. \end{cases}$$

III. AIRCRAFT DYNAMIC MODEL

The dynamic model is specifically tailored for the model-scale aircraft depicted in Fig. 2, which has a standard wing/tail configuration and a wingspan of approximately 1 m. The aircraft has a standard set of actuators constituted by two counter-rotating propellers, ailerons/flaps, elevator, and a rudder. The counter-rotating propellers provide unidirectional thrust $T \geq 0$ while keeping the induced roll negligible. The propeller's flow (slipstream) washes the wing, tail, and control surfaces, thus providing increased maneuverability during low-speed operation. In the sequel, we consider that the thrust is aligned with the wing's zero lift line and, if that is not the case, then the flaps deflection may be used to enforce such condition (at the cost of additional drag forces).

The aircraft dynamic model construction requires the definition of an inertial reference frame {I} and a body reference frame {B}, which is attached to the moving body. The reference frame {I} is fixed at some point in the Earth's surface, which is considered to be flat and still for the current application. It is identified by the set of unitary vectors {$\mathbf{i}_I, \mathbf{j}_I, \mathbf{k}_I$}, where $\mathbf{i}_I$ is directed to geographic North and is parallel to the ground, $\mathbf{k}_I$ is perpendicular to $\mathbf{i}_I$ and is directed toward the nadir, and $\mathbf{j}_I$ completes the right-handed set (this reference frame is sometimes designated by NED, or North-East-Down). The reference frame {B} is fixed at the aircraft's center of gravity and it is identified by the set of unitary vectors {$\mathbf{i}_B, \mathbf{j}_B, \mathbf{k}_B$}, where $\mathbf{i}_B$ is directed toward the aircraft nose and lies on the aircraft's symmetry plane, $\mathbf{j}_B$ is perpendicular to the aircraft's symmetry plane, and $\mathbf{k}_B$
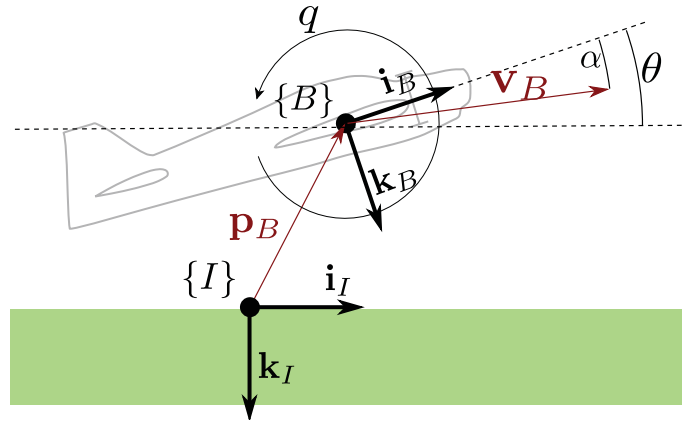

Fig. 3.   2-D representation of aircraft.

completes the right-handed set. For the sake of simplicity, we assume that $\mathbf{i}_B$ is coincident with the wing's zero-lift line and aligned with the thrust vector. This configuration of references frames is depicted in Fig. 3.

Having defined the reference frames, one obtains the aircraft equations of motion from the application of the Newton's second law to a rigid body, resulting in (see [20])

$$m\dot{\mathbf{v}} = \mathbf{f} - m\boldsymbol{\omega} \times \mathbf{v} \tag{2a}$$

$$\mathbf{I}\dot{\boldsymbol{\omega}} = \boldsymbol{\eta} - \boldsymbol{\omega} \times (\mathbf{I}\boldsymbol{\omega}) \tag{2b}$$

$$\dot{\mathbf{p}} = \mathbf{R}^\top \mathbf{v} \tag{2c}$$

$$\dot{\mathbf{R}} = -\mathbf{S}(\omega)\mathbf{R} \tag{2d}$$

where $\mathbf{v} = [u \; v \; w]^\top$ denotes the velocity of {B} w.r.t. {I} expressed in {B}, $\boldsymbol{\omega} = [p \; q \; r]^\top$ denotes the angular velocity of {B} w.r.t. {I} expressed in {B}, $\mathbf{p} = [x \; y \; z]^\top$ denotes the position of {B} w.r.t. {I} expressed in {I}, $\mathbf{R} \in SO$ (3a) and (3b) denotes the rotation matrix from {I} to {B}, $\mathbf{f} \in \mathbb{R}^3$ and $\boldsymbol{\eta} \in \mathbb{R}^3$ denote the external forces and torques acting on the aircraft, respectively, m denotes the aircraft's mass and $\mathbf{I} \in \mathbb{R}^{3\times3}$ denotes its tensor of inertia. The external forces are given by

$$\mathbf{f} = \mathbf{f}_T + \mathbf{R}\mathbf{f}_g + \mathbf{f}_a$$

where $\mathbf{f}_T = [T \; 0 \; 0]^\top$, $\mathbf{f}_g = [0 \; 0 \; mg]^\top$, and $\mathbf{f}_a = [X_a \; Y_a \; Z_a]^\top$ are the thrust, gravity, and aerodynamic forces contributions, respectively. The external moments are solely due to aerodynamic interactions, such that $\boldsymbol{\eta} = \boldsymbol{\eta}_a = [L_a \; M_a \; N_a]^\top$.

One may construct the aerodynamic forces X_a and Z_a in terms of both lift and drag as follows:

$$\begin{bmatrix} X_a \\ Z_a \end{bmatrix} = -\begin{bmatrix} \cos\alpha & -\sin\alpha \\ \sin\alpha & \cos\alpha \end{bmatrix}\begin{bmatrix} D \\ L \end{bmatrix}$$

where L denotes the wing lift, D denotes the wing drag, and $\alpha = \text{atan2}(w, u)$ is the angle of attack. The lift and drag components are described by

$$L = \frac{1}{2}\rho(u^2 + w^2)A_w C_L(\alpha) \tag{3a}$$

$$D = \frac{1}{2}\rho(u^2 + w^2)A_w C_D(\alpha) \tag{3b}$$

respectively, where $\rho \in \mathbb{R}$ is the atmospheric pressure, $A_w \in \mathbb{R}$ is the wing's planform area, $C_L(\alpha) \in \mathbb{R}$ is the coefficient of
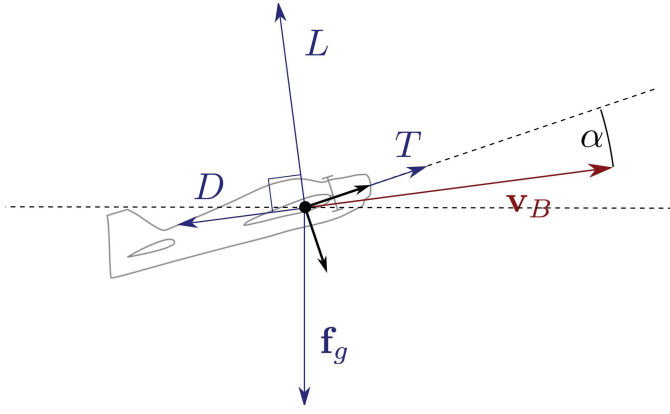
Fig. 4. Forces and moments acting on the aircraft body.

lift, and $C_D(\alpha) \in \mathbb{R}$ is the coefficient of drag (see [21] for more details). A graphical representation of these forces and moments is provided in Fig. 4.

In these computations, we have assumed that the lift and drag contributions due to the propeller slipstream are negligible due to its alignment with the wing's zero lift line. The same does not hold, however, for the aerodynamic actuators. In order to model the aerodynamic interaction between the free-stream flow and the propeller slipstream on the aerodynamic actuators, we compute both contributions separately and combine them together in the end using superposition (this strategy was successfully used in the practical setup described in [13]). We conclude that the aerodynamic torque produced by a elevator deflection $\delta_e \in \mathbb{R}$ is given by

$$M_a = x_{ac_{hs}} \frac{1}{2} \rho \Big(\|\mathbf{v}\|^2 A_{hs} \big(C_L(\alpha') \cos \alpha + C_D(\alpha') \sin \alpha \big)$$
$$+ u_p^2 A_{p,hs} C_L(\delta_e) \Big) \quad (4)$$

where $\delta_e \in \mathbb{R}$ denotes the elevator deflection, $x_{ac_{hs}}$ denotes the horizontal stabilizer's aerodynamic center, $\alpha' = \alpha + (\partial \alpha / \partial \delta_e) \delta_e$ with $(\partial \alpha / \partial \delta_e) \in \mathbb{R}$, A_{hs} denotes the horizontal stabilizer's planform area, $A_{p,hs}$ denotes the horizontal stabilizer's area which is washed by the propeller slipstream, and u_p denotes the propeller slipstream velocity. The moments L_a and N_a are related to aileron deflection δ_a and rudder deflection δ_r, respectively, in a similar way, but we omit the corresponding equations for the sake of brevity. It can be shown, using the momentum disk theory described in [22], that the propeller slipstream velocity is given by

$$u_p = \sqrt{\frac{T}{\rho A_p}}$$

where $A_p \in \mathbb{R}$ denotes the propeller disk area.

The proposed controller is intended to push the flight envelope to its limits, forcing us to build a dynamic model, which fully describes the aircraft motion for any state. One must, therefore, find the dependence of C_L and C_D over the range of all possible values for the angle of attack, i.e., $\alpha \in (-\pi, \pi]$. This constitutes a rather difficult task since, until now airplanes were not expected to fly over the stall angle and, for that reason, most literature references present airfoil

performance only for small angles of attack. However, in [23], one may find the lift and drag behaviors of symmetrical airfoils for the full angle of attack range.

For the purpose of controller design, the aircraft model is first simplified. The approximations we consider are as follows: 1) the so called "small-body forces," which denote the forces exerted on the vehicle upon the deflection of the aerodynamic actuators, are neglected (this is an usual approximation [24]); 2) Y_a is approximately zero; 3) the aerodynamic torque is considered directly as an input, but the corresponding actuator deflections are calculated with (4); 4) the thrust is readily available, i.e., the propellers' dynamics are much faster than the aircraft dynamics and can be disregarded for the purpose of controller design; and 5) the aircraft motion occurs solely on the vertical plane, i.e., $y = 0$ and

$$\mathbf{R} = \begin{bmatrix} \cos \theta & 0 & \sin \theta \\ 0 & 1 & 0 \\ -\sin \theta & 0 & \cos \theta \end{bmatrix} \quad (5)$$

where $\theta \in (-\pi, \pi]$. These approximations are verified for the particular kind of aircraft dealt with in this paper, provided that there is active regulation of the lateral movement to zero. Furthermore, notice that the controllers are designed to be robust to disturbances, which include possible model mismatches arising from these approximations.

When the aircraft motion is restricted to the vertical plane, the dynamic model (2a)–(2d) is described by the following reduced set of equations:

$$\dot{u} = \frac{X_a + T}{m} - g \sin \theta - qw + \delta_u(t) \quad (6a)$$

$$\dot{w} = \frac{Z_a}{m} + g \cos \theta + qu + \delta_w(t) \quad (6b)$$

$$\dot{q} = \frac{M_a}{\mathbf{I}_{yy}} + \delta_q(t) \quad (6c)$$

$$\dot{x} = u \cos \theta + w \sin \theta \quad (6d)$$

$$\dot{z} = -u \sin \theta + w \cos \theta \quad (6e)$$

$$\dot{\theta} = q \quad (6f)$$

where $\mathbf{I}_{yy}$ is the aircraft's moment of inertia around the body y-axis and $\delta_u(t)$, $\delta_w(t)$, and $\delta_q(t)$ are unknown perturbations which might appear due to model uncertainties, deviations from the vertical plane, sensor noise, among others.

In the sequel, we employ different Euler angle parametrizations of the rotation matrix $\mathbf{R} \in SO$ (3a) and (3b), and we use the triplet (ϕ, θ, ψ) to denote the rotations around the x-axis, y-axis, and z-axis, respectively. The usual angles employed in aircraft applications are the roll, pitch, and yaw angles, which correspond to the Z-Y-X Euler angle parametrization (see [20]). These angles, however, cannot be used to describe the aircraft attitude (5) throughout the whole flight envelope because the parametrization has singularities at $\theta = \pm \pi/2$ but the flight envelope allows for $\theta \in (-\pi, \pi]$. These parametrization issues are particularly important during the design of the lateral controllers and, for that reason, the parametrization for each operating mode is detailed in Section VI-D.

The aircraft model present in this section is valid for an aircraft of arbitrary size because the aerodynamic forces and

moments are characterized by the dimensionless quantities $C_D(\alpha)$ and $C_L(\alpha)$. These coefficients depend on the aircraft geometry and on the Reynolds number, therefore, as long as these two parameters do not change, the aircraft can be scaled arbitrarily. Since the controller is derived from the given model, it is also applicable to any aircraft which has enough thrust to overcome its weight and has enough torque to perform the transition maneuver and confine the aircraft motion to the vertical plane. These issues are addressed again in Section V, where we discuss the transition trajectory.

In the next section, we present a hybrid automaton that divides the flight envelope into four different regions, each of which is characterized by different dynamic properties.

IV. Hybrid Automaton

The previous section presented the open-loop dynamics of the aircraft system, but when several controllers are designed for different regions of the flight envelope, discrete behavior is imbued into the system due to controller switching. This behavior is better captured by means of a hybrid automaton, which is identified by: a set of the operating modes $\mathcal{Q}$; a domain mapping $\mathcal{D} : \mathcal{Q} \rightrightarrows \mathbb{R}^n \times \mathbb{R}^m$; a flow map $f : \mathcal{Q} \times \mathcal{D} \to \mathbb{R}^n$; a set of edges $\mathcal{E} \subset \mathcal{Q} \times \mathcal{Q}$; a guard mapping $\mathcal{G} : \mathcal{E} \rightrightarrows \mathbb{R}^n \times \mathbb{R}^m$ and; a reset map $\mathcal{R} : \mathcal{E} \times \mathbb{R}^n \times \mathbb{R}^m \to \mathbb{R}^n$ (see [25] for further details). The control framework presented in [15] for practical tracking of hybrid automata is used to tackle robustness issues arising from model simplifications and parametric uncertainty. This framework has been used to model UAVs interacting with the environment [26]. However, in the transition problem that we address, there are no physical obstacles inducing the operating mode jumps. Rather, the operating mode jumps depend on the topology of the controllers' basins of attraction and on the reference trajectory which is provided to the system.

In this section, we introduce a formal definition of the hybrid automaton depicted in Fig. 5. The definition relies heavily on the properties of the controllers designed for each operating mode; therefore, it is important to introduce some of those properties beforehand. The controller of the operating mode $q \in \mathcal{Q}$ is the map

$$(t, \boldsymbol{\xi}) \mapsto \boldsymbol{\mu}_q(t, \boldsymbol{\xi})$$

and it has a basin of attraction (possibly time-varying) $\mathcal{B}_q(\boldsymbol{\xi}^\star(t), \boldsymbol{\mu}^\star(t)) \subset \mathbb{R}^6 \times \mathbb{R}^2$, as defined below.

Definition 1: Let $\boldsymbol{\phi}(t, \boldsymbol{\xi})$ be the solution to $\dot{\boldsymbol{\xi}} = f(q, \boldsymbol{\xi}, \boldsymbol{\mu}_q)$, for some $q \in \mathcal{Q}$, that starts at initial state $\boldsymbol{\xi}$ and is defined for all $t \geq 0$. The basin of attraction of the operating mode $q \in \mathcal{Q}$ is

$$
\mathcal{B}_q(\boldsymbol{\xi}^\star(t), \boldsymbol{\mu}^\star(t)) = \Big\{ (\boldsymbol{\xi}, \boldsymbol{\mu}) \in \mathbb{R}^6 \times \mathbb{R}^2 : \lim_{t \to \infty} (\boldsymbol{\phi}(t, \boldsymbol{\xi}), \boldsymbol{\mu})
$$
$$
= (\boldsymbol{\xi}^\star(t), \boldsymbol{\mu}^\star(t)), \boldsymbol{\mu} = \boldsymbol{\mu}_q(t, \boldsymbol{\phi}(t, \boldsymbol{\xi})) \Big\}. \quad (7)
$$

$\square$

For the particular application of performing a transition between hover and level, the individual operative mode controllers, whose development is deferred to Section VI, have the following properties: the hover controller $\boldsymbol{\mu}_H$ stabilizes the
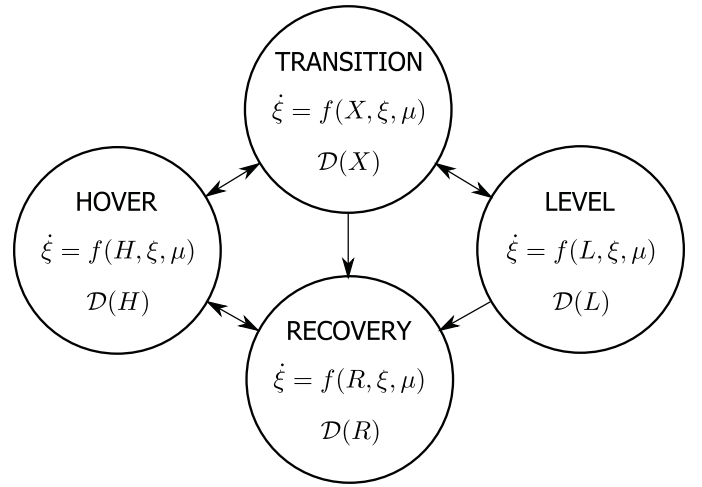

Fig. 5. System's hybrid automaton. The formal description of the hybrid automaton includes the definition of the domain $\mathcal{D}(q)$, the flow map $f(q, \boldsymbol{\xi}, \boldsymbol{\mu})$, the edges $\mathcal{E} \subset \mathcal{Q} \times \mathcal{Q}$, the guard map $\mathcal{G}(\mathcal{E})$, and the reset map $\mathcal{R}(\mathcal{E}, \boldsymbol{\xi}, \boldsymbol{\mu})$ for each operating mode $q \in \mathcal{Q}$, provided in the sequel.

aircraft at a given trimming trajectory $(\boldsymbol{\xi}_{H_{\mathrm{eq}}}, \boldsymbol{\mu}_{H_{\mathrm{eq}}})$ with basin of attraction $\mathcal{B}_H(\boldsymbol{\xi}_{H_{\mathrm{eq}}}, \boldsymbol{\mu}_{H_{\mathrm{eq}}})$, the level controller $\boldsymbol{\mu}_L$ stabilizes the aircraft at a given trimming trajectory $(\boldsymbol{\xi}_{L_{\mathrm{eq}}}, \boldsymbol{\mu}_{L_{\mathrm{eq}}})$ with basin of attraction $\mathcal{B}_L(\boldsymbol{\xi}_{L_{\mathrm{eq}}}, \boldsymbol{\mu}_{L_{\mathrm{eq}}})$, and the transition controller $\boldsymbol{\mu}_X$ performs practical tracking of a reference trajectory with an error no larger than $\epsilon > 0$. In order to be consistent with the notation introduced in [15], the reference trajectories are denoted by

$$v_{q_1 \to q_2}^\star(t) = (\boldsymbol{\xi}_{q_1 \to q_2}^\star(t), \boldsymbol{\mu}_{q_1 \to q_2}^\star(t))$$

for all $t \geq 0$ and for some suitable pair $(q_1, q_2) \in \mathcal{E}$. Additional details on the design of the reference trajectories are provided in Section V; the recovery controller performs stabilization of the hover trimming trajectory and it has a basin of attraction $\mathcal{B}_R(\boldsymbol{\xi}_{H_{\mathrm{eq}}}, \boldsymbol{\mu}_{H_{\mathrm{eq}}})$ which one wants to make as large as possible. Ideally, $\mathcal{B}_R(\boldsymbol{\xi}_{H_{\mathrm{eq}}}, \boldsymbol{\mu}_{H_{\mathrm{eq}}}) = \mathbb{R}^6 \times \mathbb{R}^2$. In practice, it is very difficult to determine the topology of the basins of attraction for nonlinear systems. Nevertheless, Lyapunov functions can be used to provide estimates of the basins of attraction, using some conservative bounds which allow this task to become slightly easier [27, Corollary 1].

For the Hybrid Automaton describing the airplane system, we consider the system state $\boldsymbol{\xi} \in \mathbb{R}^6$ and the actuator input $\boldsymbol{\mu} \in \mathbb{R}^2$ are given by

$$\boldsymbol{\xi} = [u \; w \; q \; \theta \; x \; z]^\top$$
$$\boldsymbol{\mu} = [\tau_u \; \tau_q]^\top$$

where $\tau_u = T/m$, $\tau_q = M_a/J$. A graphical representation of the automaton is presented in Fig. 5 and a detailed description follows in the sequel.

In the following paragraphs, we describe the hybrid automaton presented in Fig. 5 in detail.

1) Operating Modes: The operating mode q belongs to the set $\mathcal{Q} = \{H, L, X, R\}$, where H is the hover operating mode, X is the transition operating mode, L is the level operating mode, and R is the recovery operating mode.

2) Edges: The set of edges $\mathcal{E} \subset \mathcal{Q} \times \mathcal{Q}$ identifies any operating mode transition from q_1 to q_2 represented in Fig. 5 with the pair (q_1, q_2). The possible operating mode transitions in this model are: (H, X), (X, L), (L, X), (X, H), (H, R), (X, R), (L, R), and (R, H).

3) Domain Mapping: For each operating mode, the domain mapping $\mathcal{D} : \mathcal{Q} \rightrightarrows \mathbb{R}^6 \times \mathbb{R}^2$ assigns the set where the variables $(\boldsymbol{\xi}, \boldsymbol{\mu})$ may range and it is defined by

$$\mathcal{D}(H) = \mathcal{B}_H(\boldsymbol{\xi}_{H_{eq}}, \boldsymbol{\mu}_{H_{eq}})$$
$$\mathcal{D}(X) = \mathcal{B}_X(\boldsymbol{\xi}^\star_{q_1 \to q_2}(t), \boldsymbol{\mu}^\star_{q_1 \to q_2}(t))$$
$$\mathcal{D}(L) = \mathcal{B}_L(\boldsymbol{\xi}_{L_{eq}}, \boldsymbol{\mu}_{L_{eq}})$$
$$\mathcal{D}(R) = \mathcal{B}_R(\boldsymbol{\xi}_{H_{eq}}, \boldsymbol{\mu}_{H_{eq}})$$

where $v^\star_{q_1 \to q_2}(t) = (\boldsymbol{\xi}^\star_{q_1 \to q_2}(t), \boldsymbol{\mu}^\star_{q_1 \to q_2}(t))$ is a given reference trajectory defined for all $t \geq t_0$.

4) Flow Map: The flow map $f : \mathcal{Q} \times \mathbb{R}^6 \times \mathbb{R}^2 \to \mathbb{R}^6$ describes the evolution of the state variables in each operating mode $q \in \mathcal{Q}$, i.e., in each operating mode, the state's derivative is given by

$$\dot{\boldsymbol{\xi}} = f(q, \boldsymbol{\xi}, \boldsymbol{\mu})$$

where function f is derived from the differential equations (6) and $q \in \mathcal{Q}$ only affects the choice of the controller.

5) Guard Mapping: The guard mapping $\mathcal{G} : \mathcal{E} \rightrightarrows \mathbb{R}^6 \times \mathbb{R}^2$ determines, for each pair $(q_1, q_2) \in \mathcal{E}$, the set to which the aircraft state must belong in order to perform the transition from q_1 to q_2. The rationale behind the Guard mapping design is as follows. The hover and level controllers stabilize (6) in a neighborhood of their respective trimming trajectories and, additionally, the transition controller performs the tracking of a reference trajectory between these two (disjoint) regions with arbitrarily small error $\epsilon > 0$. The Guard mapping design guarantees the stability of the overall system under nominal operation, because controller switching occurs only when the system state is (robustly) inside the stable regions of the hover and level trimming trajectories. If the system state is driven outside this stability region due to unexpected perturbations, then the recovery controller is triggered. These considerations are encoded in the following definition of the guard map:

$$\mathcal{G}(H, X) = B_{\epsilon_0}(v^\star_{q_1 \to q_2}(0))$$
$$\mathcal{G}(X, L) = B_{\underline{l}}(\boldsymbol{\xi}_{L_{eq}}, \boldsymbol{\mu}_{L_{eq}})$$
$$\mathcal{G}(L, X) = B_{\epsilon_0}(v^\star_{q_1 \to q_2}(0))$$
$$\mathcal{G}(X, H) = B_{\underline{h}}(\boldsymbol{\xi}_{H_{eq}}, \boldsymbol{\mu}_{H_{eq}})$$
$$\mathcal{G}(H, R) = \mathbb{R}^8 \backslash B_{\overline{h}}(\boldsymbol{\xi}_{H_{eq}}, \boldsymbol{\mu}_{H_{eq}})$$
$$\mathcal{G}(L, R) = \mathbb{R}^8 \backslash B_{\overline{l}}(\boldsymbol{\xi}_{L_{eq}}, \boldsymbol{\mu}_{L_{eq}})$$
$$\mathcal{G}(X, R) = \mathbb{R}^8 \backslash B_{\epsilon}(v^\star_{q_1 \to q_2}(t))$$
$$\mathcal{G}(R, H) = B_{\underline{h}}(\boldsymbol{\xi}_{H_{eq}}, \boldsymbol{\mu}_{H_{eq}})$$

where $\epsilon_0 > 0$ is the maximum allowed error on the initial state of a transition maneuver, $B_{\underline{l}}(\boldsymbol{\xi}_{L_{eq}}, \boldsymbol{\mu}_{L_{eq}}) \subset B_{\overline{l}}(\boldsymbol{\xi}_{L_{eq}}, \boldsymbol{\mu}_{L_{eq}}) \subset \mathcal{B}_L(\boldsymbol{\xi}_{L_{eq}}, \boldsymbol{\mu}_{L_{eq}})$ and similarly $B_{\underline{h}}(\boldsymbol{\xi}_{H_{eq}}, \boldsymbol{\mu}_{H_{eq}}) \subset B_{\overline{h}}(\boldsymbol{\xi}_{H_{eq}}, \boldsymbol{\mu}_{H_{eq}}) \subset \mathcal{B}_H(\boldsymbol{\xi}_{H_{eq}}, \boldsymbol{\mu}_{H_{eq}})$, with $\underline{l}, \overline{l} \in \mathbb{R}$ and $\underline{h}, \overline{h} \in \mathbb{R}$. The parameters $\underline{h}, \overline{h}, \underline{l}$, and $\overline{l}$ are chosen so as to prevent chattering during switching events, which is always possible by choosing $\underline{h} < \overline{h}$ and $\underline{l} < \overline{l}$ sufficiently apart from
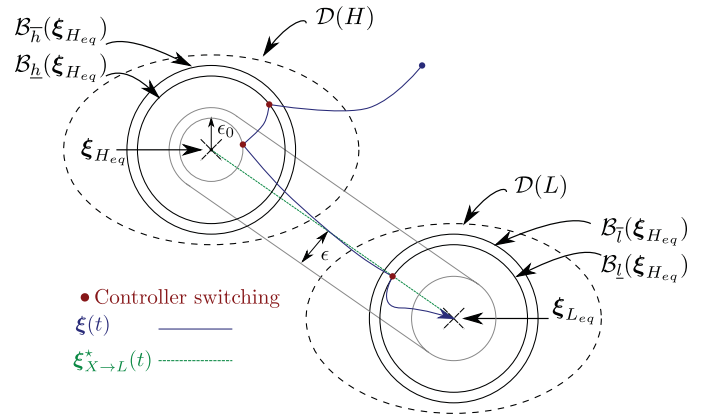

Fig. 6. Hybrid automaton sample trajectory. The aircraft starts in recovery mode with $q^\star = L$, switches to hover when $(\boldsymbol{\xi}, \boldsymbol{\mu}) \in B_{\underline{h}}(\boldsymbol{\xi}_{H_{eq}}, \boldsymbol{\mu}_{H_{eq}})$ and to transition when $\boldsymbol{\xi} \in B_{\epsilon_0}(v^\star_{X \to L}(0))$. In the end, the aircraft switches to level when $(\boldsymbol{\xi}, \boldsymbol{\mu}) \in B_{\underline{l}}(\boldsymbol{\xi}_{L_{eq}}, \boldsymbol{\mu}_{L_{eq}})$.

each other. Fig. 6 depicts these sets for a sample trajectory, from the recovery to the level operating mode.

6) Reset Map: For each $(q_1, q_2) \in \mathcal{E}$ and $(\xi, \mu) \in \mathcal{G}(q_1, q_2)$, the reset map $\mathcal{R} : \mathcal{E} \times \mathbb{R}^6 \times U \to \mathbb{R}^6$ identifies the jump of the state variable ξ during the operating mode transition from q_1 to q_2. For this particular application, the reset map is the trivial map

$$\mathcal{R}(\{q_1, q_2\}, \xi, \mu) = \xi \text{ for any } \{q_1, q_2\} \in \mathcal{E}$$

as there are no impulsive state changes, only the employed local controller is modified when switching operating modes.

V. ROBUST MANEUVERS

The problem of achieving robust transitions between hover and level flights is twofold: 1) the reference maneuver which links the two sets must be at least ϵ-distant from the domain limits and any guard sets leading to undesired operative mode transitions and 2) the controller must be able to achieve practical reference trajectory tracking with an error no larger than ϵ, in the presence of external disturbances and uncertain parameters.

Three different kinds of robust maneuvers are defined within the followed Hybrid Automata control framework [15]. The first one, denoted as ϵ-robust q_1-single maneuver in $[t_0, t_1]$, is such that the state and the input do not intersect any guard condition in order to maintain the same "single" operating mode q_1. The second type, denoted as ϵ-robust $q_1 \to q_2$ approach maneuver in $[t_0, t_f]$, is such that at time t_f the maneuver belongs robustly to the desired guard set, $\mathcal{G}(\{q_1, q_2\})$, in order to guarantee a switch to the operating mode q_2. The last one, the $q_1 \to q_2$ transition maneuver in $[t_0, t_1]$, is obtained as a combination of an ϵ-robust $q_1 \to q_2$ approach maneuver and a set of ϵ-robust q_2-single maneuvers.

Although q_1-single maneuvers and $q_1 \to q_2$ transition maneuvers are defined for the hybrid automaton presented in Section IV, the most important maneuvers are the $X \to L$ and $X \to H$ approach maneuvers, identified by $v^\star_{X \to L}(t)$ and $v^\star_{X \to H}(t)$, respectively. These reference maneuvers are

computed by means of nominal system inversion. The nominal system is given by (6) and may be rewritten as

$$\dot{u} = \tau_u + h_u(u, w, q, \theta)$$
$$\dot{w} = h_w(u, w, q, \theta)$$
$$\dot{q} = \tau_q$$
$$\dot{\theta} = q \qquad (8)$$

where

$$h_u(u, w, q, \theta) = \frac{X_a}{m} - g \sin\theta - qw$$
$$h_w(u, w, q, \theta) = \frac{Z_a}{m} + g \cos\theta + qu$$

and $\delta_u(t) = \delta_w(t) = \delta_q(t) = 0$. Given twice differentiable desired state trajectories $u^\star(t)$ and $\theta^\star(t)$, the downward velocity initial state $w^\star(0)$, then the reference control inputs $\tau_u^\star(t)$ and $\tau_q^\star(t)$, and the reference state variable $w^\star(t)$ are computed numerically by solving (8).

The design of optimal transition maneuvers between hovered and leveled flight for aerial vehicles is an active research topic by itself, as can be seen in [28]–[30], and does not constitute the main focus of this paper. Instead, we design the transition trajectories using some intuitive insight mentioned in [28]–[30]: 1) the transition maneuver connects the hover and the level trimming trajectories, denoted by $(\boldsymbol{\xi}_{H_{eq}}, \boldsymbol{\mu}_{H_{eq}})$ and $(\boldsymbol{\xi}_{L_{eq}}, \boldsymbol{\mu}_{L_{eq}})$, respectively; 2) the propeller's maximum thrust must overcome the weight of the aircraft by, at least, an amount $\nu_T > 0$ in order to perform any transition trajectories, i.e., $T_{max} > (1 + \nu_T)mg$ (it is suggested in [29] that $\nu_T \geq 0.15$); 3) as a safe trajectory design guideline, we exploited trajectories where the angle of attack was constrained to small values, typically $|\alpha| < 15°$; 4) the reference trajectory must have the property that $u^\star(t) > 0$ for all $t \geq t_0$; and 5) the maximum torque during the transition maneuver should verify $\tau_q(t) \leq \nu_M$, for some $\nu_M > 0$ and for all $t \geq t_0$.

The chosen reference trajectories are smooth functions which are characterized by the initial forward velocity u_0, the final forward velocity u_∞, the initial pitch angle θ_0, the final pitch angle θ_∞, the transition start times t_θ, and t_u and the parameters Φ_u and Φ_θ which determine the speed at which the transition is performed for each of the state variables u and θ. The selected parameters provide faster transient in the forward velocity u than in the pitch angle θ during the transition from hovered to leveled flight, in order to increase maneuverability. The transition from level flight to hover is simply a pitch up maneuver at constant forward speed. This speed is only brought to zero when the aircraft is facing the zenith. The transition maneuvers are defined by

$$u^\star(t) = \begin{cases} u_0, & \text{if } t_0 \leq t < t_u \\ u_0 + (u_\infty - u_0)\exp(-\Phi_u(t - t_u)) \\ \quad (\exp(\Phi_u(t - t_u)) - \Phi_u(t - t_u) - 1), & \text{if } t \geq t_u \end{cases}$$

$$\theta^\star(t) = \begin{cases} \theta_0, & \text{if } t_0 \leq t < t_\theta \\ \theta_0 + (\theta_\infty - \theta_0)\exp(-\Phi_\theta(t - t_\theta)) \\ \quad (\exp(\Phi_\theta(t - t_\theta)) - \Phi_\theta(t - t_\theta) - 1), & \text{if } t \geq t_\theta. \end{cases}$$

These trajectories are used for hover to level flight and level flight to hover transitions with appropriate parameter choice.
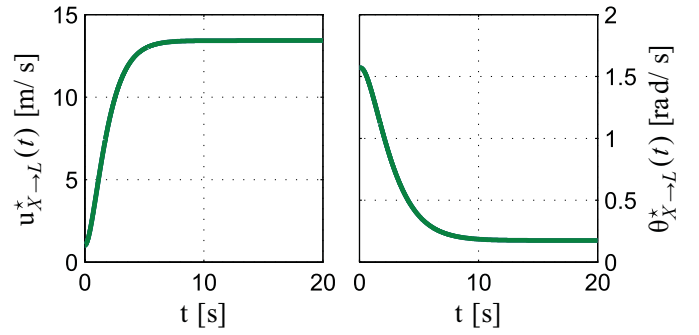

Fig. 7. Reference trajectory $(u^\star, \theta^\star)$ for the transition maneuver from hover to level, with $u_0 = 1$ m/s, $u_\infty = 10.83$ m/s, $\Phi_u = 1$ s^{-1}, $t_u = 0$ s, $\theta_0 = 90°$, $\theta_\infty = 10°$, $\Phi_\theta = 0.7$ s^{-1}, and $t_\theta = 0.1$ s.

The same strategy can be employed for aircrafts with different sizes, as long as the conditions $\tau_{u_{max}} > (1 + \nu_T)g$ and $\tau_{q_{max}} > \nu_M$ are verified. These conditions, however, are very naive and it might be very difficult to verify them for larger scale aircrafts, if not impossible. As a general rule, the aircraft designer should know that scaling up the aircraft without any other changes will lead to slower transition trajectories and less hovering time. Therefore, there is an upper bound on the aircraft scale where the proposed strategy may still be applied. Partial solutions to this problem include the change to fuel with higher energy density and improved aircraft geometry.

A sample reference trajectory from hover to level is depicted in Fig. 7 for the following parameters: $u_0 = 1$ m/s, $u_\infty = 10.83$ m/s, $\Phi_u = 1$ s^{-1}, $t_u = 0$ s, $\theta_0 = 90°$, $\theta_\infty = 10°$, $\Phi_\theta = 0.7$ s^{-1}, and $t_\theta = 0.1$ s.

VI. CONTROLLER DESIGN

The Hybrid Automaton's definition provided in Section IV requires the design of four controllers, one for each operating mode. Summarizing the previously stated requirements, the controller objectives are to: 1) robustly stabilize the aircraft in hovered and leveled flights; 2) perform the tracking of a given reference trajectory, which takes the aircraft from hover to level and vice-versa with a tracking error no larger than ϵ; 3) whenever the aircraft state overcomes some specified bounds, perform a recovery maneuver which takes the aircraft to hover and is robust with respect to exogenous disturbances; and 4) design a controller for each operating mode, which stabilizes the lateral motion of the aircraft, thus keeping it on the vertical plane. Such diversity of control objectives requires the application of different control laws to each operating mode.

In hovered and leveled flights, we adopt a linear control law of the form $\tilde{\boldsymbol{\mu}}_q = -\mathbf{K}\tilde{\boldsymbol{\xi}}_q$, where $\tilde{\boldsymbol{\xi}}_q = \boldsymbol{\xi} - \boldsymbol{\xi}_q^\star$ is the error between the state and some constant reference $\boldsymbol{\xi}_q^\star$, and the state feedback gain $\mathbf{K}$ is computed as the solution to an optimal control problem subject to linear matrix inequalities constraints (in the computations, we used the openly available YALMIP Toolbox [31]). A nonlinear controller which performs reference tracking is employed during transition operating mode and another nonlinear controller which renders the hover equilibrium point globally stable is used while in recovery mode. For the lateral controller, we employ scheduled

controller gains using a similar strategy to that which is used in the hover and level controllers design. Each of the proposed solutions is further detailed in the sequel.

In addition, one needs to be careful about input saturations because it imposes severe constraints on the control. The reader must keep in mind that $\boldsymbol{\mu}_q(t) \in U \subset \mathbb{R}^2$, where

$$U = [\tau_{u_{\min}}, \tau_{u_{\max}}] \times [\tau_{q_{\min}}, \tau_{q_{\max}}].$$

The controller design presented in Section VI may not address this issue explicitly, but the controller design parameters, the reference trajectory, and the hybrid automaton's definition are tuned to prevent the boundaries of the actuators from being reached.

A. Hover and Level Controllers

To design the hover and level flight controllers, we use a gain scheduling control methodology. A bank of linear controllers is designed for different operative conditions, and the closed-loop controller to be used is dependent on the vehicle state. The scheduling of the different controllers is achieved without discontinuities in the output by using the D-methodology. See [32] and [33] for an application of the same technique to the automated level flight and landing of an aircraft.

Consider the LPV system

$$\dot{\tilde{\boldsymbol{\xi}}} = \mathbf{A}(\delta)\tilde{\boldsymbol{\xi}} + \mathbf{B}(\delta)\tilde{\boldsymbol{\mu}} \tag{9}$$

which approximates the nonlinear system (6) within a known region $\delta \in \Delta$. The hover and level operating mode controllers are obtained as the solution to the optimal control problem of minimizing the cost function

$$J = \int_0^\infty \tilde{\boldsymbol{\xi}}^\top \mathbf{Q}\tilde{\boldsymbol{\xi}} + \tilde{\boldsymbol{\mu}}^\top \mathbf{R}\tilde{\boldsymbol{\mu}} \, \mathrm{d}t. \tag{10}$$

In addition to the approximation of the general nonlinear model as a LPV system, we select the polytopic LPV structure which is defined below.

Definition 2: System (9) is said to be a polytopic LPV system with affine parameter dependence if the system matrix

$$\mathbf{S}(\delta) = [\mathbf{A}(\delta) \ \mathbf{B}(\delta)]$$

verifies $\mathbf{S}(\delta) = \mathbf{S}_0 + \mathbf{S}_\delta \delta$, for all $\delta \in \Delta$, and the parameter set takes the form $\Delta = \mathrm{co}(\Delta_0)$, where Δ_0 is a set with a finite number of points, i.e., $\Delta_0 = \{\delta_1, \ldots, \delta_r\}$.

In a polytopic LPV setting, the solution to the minimization of (10) results in a linear control feedback law of the form

$$\tilde{\boldsymbol{\mu}}_q = -\mathbf{K}\tilde{\boldsymbol{\xi}}_q. \tag{11}$$

Additionally, the polytopic formulation enables the stability assessment of the solutions to (9) by solving a finite set of linear matrix inequalities [34]. The control objective is translated into the following optimization problem:

$$\begin{aligned} \min \quad & \mathrm{tr}(\mathbf{P}) \\ \mathrm{s.t.} \quad & \mathbf{A}(\delta_i)^\top \mathbf{P} + \mathbf{P}\mathbf{A}(\delta_i) + \mathbf{K}^\top \mathbf{B}(\delta_i)^\top \mathbf{P} + \mathbf{P}\mathbf{B}(\delta_i)\mathbf{K} \\ & < -\mathbf{Q} - \mathbf{K}^\top \mathbf{R}\mathbf{K} \end{aligned} \tag{12}$$

for all $\delta_i \in \Delta_0$. It can be shown using the Schur's complement and the congruence transformations $\mathbf{Y} = \mathbf{P}^{-1}$ and $\mathbf{L} = \mathbf{KY}$, that the previous optimization problem is equivalent to

$$\begin{aligned} \max \quad & \mathrm{tr}(\mathbf{Y}) \\ \mathrm{s.t.} \quad & \begin{bmatrix} \mathbf{YA}(\delta_i)^\top + \mathbf{A}(\delta_i)\mathbf{Y} + \mathbf{L}^\top \mathbf{B}(\delta_i)^\top + \mathbf{B}(\delta_i)\mathbf{L} & \mathbf{Y} & \mathbf{L}^\top \\ \mathbf{Y} & -\mathbf{Q}^{-1} & 0 \\ \mathbf{L} & 0 & -\mathbf{R}^{-1} \end{bmatrix} < 0 \\ & -\mathbf{Q}^{-1} < 0 \\ & -\mathbf{R}^{-1} < 0 \end{aligned}$$

for all $\delta_i \in \Delta_0$.

The following result shows that the feedback controller stabilizes the LPV system (9) for all $\delta \in \Delta$.

Proposition 3: Consider the LPV system (9) and the control law (11), where $\mathbf{K}$ is a solution to (12), then the closed-loop system is globally asymptotically stable for all $\delta \in \Delta$.

Proof: Consider the Lyapunov function candidate

$$V = \tilde{\boldsymbol{\xi}}^\top \mathbf{P}\tilde{\boldsymbol{\xi}}$$

whose derivative is given by

$$\dot{V} = \tilde{\boldsymbol{\xi}}^\top (\mathbf{A}(\delta)\mathbf{P} + \mathbf{P}\mathbf{A}(\delta) + \mathbf{K}^\top \mathbf{B}^\top(\delta)\mathbf{P} + \mathbf{P}\mathbf{B}(\delta)\mathbf{K})\tilde{\boldsymbol{\xi}}.$$

Since $\mathbf{K}$ satisfies (12), the Lyapunov function's derivative is upper bounded by

$$\dot{V} = -\tilde{\boldsymbol{\xi}}^\top (\mathbf{Q} + \mathbf{K}^\top \mathbf{R}\mathbf{K})\tilde{\boldsymbol{\xi}} < 0$$

therefore, global asymptotic stability follows by standard Lyapunov arguments. ∎

Each operating mode has a different operating point and specifications which require distinct weightings. Therefore, controller dimensioning requires:

1) linearization around the chosen operating point $(\boldsymbol{\xi}_q, \boldsymbol{\mu}_q)$;
2) integrator states choice according to the operating mode requirements;
3) controllability evaluation;
4) $(\mathbf{Q}, \mathbf{R})$ weighting using Bryson's trial-and-error method, [35], which employs the diagonal matrices

$$\mathbf{Q} = \begin{bmatrix} \Delta\boldsymbol{\xi}_{1_{\max}}^{-2} & \cdots & 0 \\ \vdots & \ddots & \vdots \\ 0 & \cdots & \Delta\boldsymbol{\xi}_{n_{\max}}^{-2} \end{bmatrix}$$

$$\mathbf{R} = \begin{bmatrix} \Delta\boldsymbol{\mu}_{1_{\max}}^{-2} & \cdots & 0 \\ \vdots & \ddots & \vdots \\ 0 & \cdots & \Delta\boldsymbol{\mu}_{m_{\max}}^{-2} \end{bmatrix}$$

where $\Delta\boldsymbol{\xi}_{i_{\max}}$ represents the ith state maximum expected deviation from equilibrium and $\Delta\boldsymbol{\mu}_{j_{\max}}$ represents the jth input maximum expected deviation from equilibrium.

The proposed controllers stabilize the simplified aircraft system (9) if $\delta(t) \in \Delta$ for all $t \geq 0$. This provides some information about the size of the basin of attraction $\mathcal{B}_q(\boldsymbol{\xi}_{q_{\mathrm{eq}}}, \boldsymbol{\mu}_{q_{\mathrm{eq}}})$ for each $q \in \{H, L\}$. The set Δ depends on the parameters $\boldsymbol{\delta}_q = [\tilde{u}_q \ \tilde{\theta}_q]^\top$. The admissible ranges for these parameters are

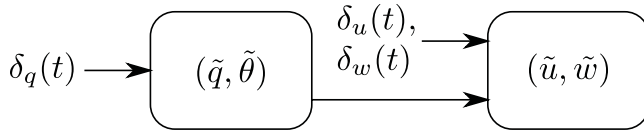$$\tilde{u} \in [\tilde{u}_{q_{\min}}, \tilde{u}_{q_{\max}}]$$

Fig. 8.   Transition cascade system representation.

$$\tilde{\theta} \in [\tilde{\theta}_{q\min}, \tilde{\theta}_{q\max}]. \tag{13}$$

The LPV system approximation is performed using a least square fitting to the nonlinear system, upon linearization within a denser grid with the limits defined by (13). The extent of the simplifications made so far depend on the size of the set Δ and on the deviations between the LPV and the nonlinear systems.

B. Transition Controller

The controller for the transition operating mode provides practical tracking of a reference trajectory $v^\star(t) = (u^\star(t), w^\star(t), q^\star(t), \theta^\star(t), \tau_u^\star(t), \tau_q^\star(t))$, computed according to the criteria defined in Section V. Using the error variables $\tilde{u} = u - u^\star(t)$, $\tilde{w} = w - w^\star(t)$, $\tilde{q} = q - q^\star(t)$, and $\tilde{\theta} = \theta - \theta^\star(t)$, we will prove that there exist positive gains k_u, k_q, and k_θ such that the feedback control law

$$\boldsymbol{\mu}_X = \begin{bmatrix} \tau_u^\star(t) + \tilde{\tau}_u \\ \tau_q^\star(t) + \tilde{\tau}_q \end{bmatrix} \tag{14}$$

with

$$\tilde{\tau}_u = -k_u \tilde{u}$$
$$\tilde{\tau}_q = -k_\theta(\tilde{\theta} + k_q \tilde{q})$$

locally asymptotically stabilizes the error dynamics, given by

$$\dot{\tilde{u}} = \tilde{\tau}_u + \Psi_u(\tilde{u}, \tilde{w}, \tilde{q}, \tilde{\theta}, t) + \delta_u(t) \tag{15a}$$
$$\dot{\tilde{w}} = \Psi_w(\tilde{u}, \tilde{w}, \tilde{q}, \tilde{\theta}, t) + \delta_w(t) \tag{15b}$$
$$\dot{\tilde{q}} = \tilde{\tau}_q + \delta_q(t) \tag{15c}$$
$$\dot{\tilde{\theta}} = \tilde{q} \tag{15d}$$

where

$$\Psi_u(\tilde{u}, \tilde{w}, \tilde{q}, \tilde{\theta}, t) = h_u(u^\star(t) + \tilde{u}, w^\star(t) + \tilde{w}, q^\star(t) + \tilde{q}, \theta + \tilde{\theta})$$
$$- h_u(u^\star(t), w^\star(t), q^\star(t), \theta^\star(t))$$
$$\Psi_w(\tilde{u}, \tilde{w}, \tilde{q}, \tilde{\theta}, t) = h_w(u^\star(t) + \tilde{u}, w^\star(t) + \tilde{w}, q^\star(t) + \tilde{q}, \theta + \tilde{\theta})$$
$$- h_w(u^\star(t), w^\star(t), q^\star(t), \theta^\star(t)). \tag{16}$$

The reference trajectory is one of equilibrium (if $\delta_u = \delta_w = \delta_q = 0$) because

$$[\tilde{u}\ \tilde{w}\ \tilde{q}\ \tilde{\theta}] = [0\ 0\ 0\ 0] \Rightarrow [\dot{\tilde{u}}\ \dot{\tilde{w}}\ \dot{\tilde{q}}\ \dot{\tilde{\theta}}] = [0\ 0\ 0\ 0].$$

Consider two cascade systems depicted in Fig. 8, which describe the dynamics of $(\tilde{u}, \tilde{w})$ and $(\tilde{q}, \tilde{\theta})$. Input-to-state stability is established separately for each of these systems in Propositions 4 and 6, from which input-to-state stability for the overall system then follows.

Due to the underactuation of (15), it is important to study the properties of the function $\Psi_w(\tilde{u}, \tilde{w}, \tilde{q}, \tilde{\theta}, t)$, which characterizes the dynamics around the equilibrium trajectory for

the state variable $w \in \mathbb{R}$. Employing the Taylor's polynomial expansion around $\tilde{w} = 0$ yields

$$\Psi_w(\tilde{u}, \tilde{w}, \tilde{q}, \tilde{\theta}, t) = \Psi_w|_{\tilde{w}=0} + R_0(\tilde{w}) \tag{17}$$

where $R_0(\tilde{w})$ is the remainder, satisfying

$$\lim_{\tilde{w} \to 0} |R_0(\tilde{w})| = 0$$

according to Taylor's theorem [36]. Moreover, $R_0(\tilde{w})$ is given by

$$R_0(\tilde{w}) = \left. \frac{\partial \Psi_w}{\partial \tilde{w}} \right|_{\tilde{w}=\tilde{w}_0} \tilde{w}$$

for some $\tilde{w}_0 \in [0, \tilde{w}]$. The first order partial derivative of $\Psi_w(\tilde{u}, \tilde{w}, \tilde{q}, \tilde{\theta}, t)$ with respect to $\tilde{w}$ is given by

$$\frac{\partial \Psi_w}{\partial \tilde{w}} = -\frac{1}{2}\rho A \sqrt{u^2 + w^2}\delta(\alpha) \tag{18}$$

with

$$\delta(\alpha) = C_D(\alpha)(1 + \sin^2(\alpha))$$
$$+ \frac{1}{2}\left(C_L(\alpha) + \frac{\partial C_D(\alpha)}{\partial \alpha}\right)\sin(2\alpha)$$
$$+ \frac{\partial C_L(\alpha)}{\partial \alpha}\cos^2(\alpha). \tag{19}$$

This derivative plays a crucial role on the stability of the closed-loop system as argued in Proposition 4. In particular, one must design a reference trajectory from the hover domain to the level domain such that $\delta(\alpha^\star(t)) > 0$ for all $t \geq 0$, where

$$\alpha^\star(t) = \text{atan2}(w^\star(t), u^\star(t)).$$

Assuming that the lift and drag coefficients are described by

$$C_L(\alpha) = C_{L_\alpha}\alpha$$
$$C_D(\alpha) = C_{D_0} + kC_L(\alpha)^2 \tag{20}$$

for some $C_{L_\alpha} > 0$, $C_{D_0} > 0$ and $k > 0$ (see [21]), then it is straightforward to show that there exist such trajectories for small enough $\alpha^\star(t)$, since we have $\delta(0) = C_{L_\alpha} > 0$. Equation (20) is only applicable for small angles of attack which is somewhat limiting for the application we are considering. If we assume that the lift and drag profiles are given by

$$C_L = C_{L_0}\sin(2\alpha)$$
$$C_D = C_{D_0} + C_{D_1}\sin^2(\alpha) \tag{21}$$

for the whole range of angles of attack, then it is possible to verify that $\delta(\alpha) > 0$ holds for all $\alpha \in (-\pi, \pi]$ (see Fig. 9). From Fig. 10, one may check that (21) is a reasonable approximation but it hides the issue of airfoil stall, which is indeed a very important factor affecting the behavior of $\delta(\alpha)$ because, at that point, the term $(\partial C_L(\alpha)/\partial \alpha)\cos^2(\alpha)$ becomes negative due to the loss of lift.

A lift profile which models the stall behavior is provided in [37], and it is given by

$$C_L(\alpha) = (1 - \chi(\alpha))(C_{L_0} + C_{L_\alpha}\alpha)$$
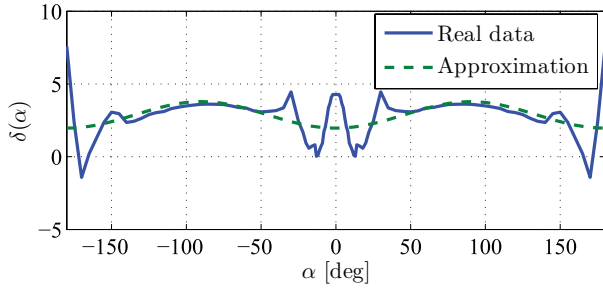$$+ \chi(\alpha)(2\text{sign}(\alpha)\sin^2(\alpha)\cos(\alpha))$$

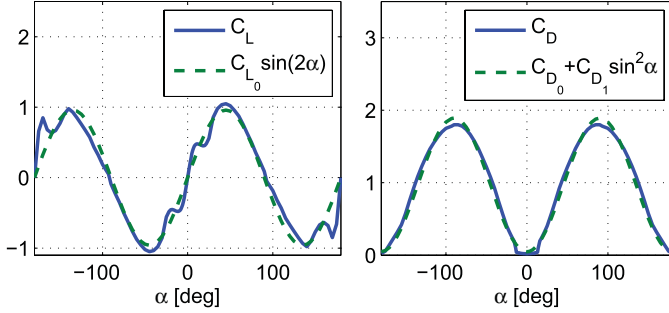Fig. 9. $\delta(\alpha)$ for the NACA0025 airfoil at Re = 80 000 [23], using real data and the approximation (21).

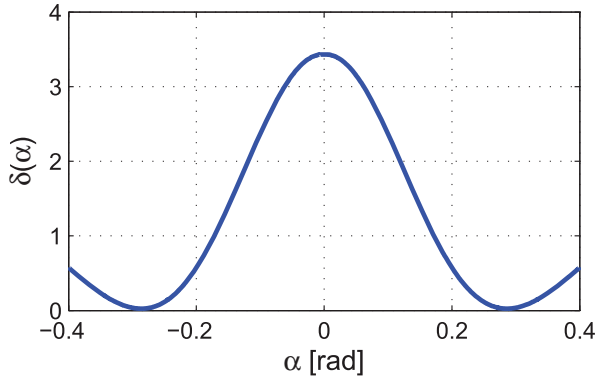Fig. 10. NACA0025 airfoil data at Re = 80 000 [23].

Fig. 11. Parameter $\delta(\alpha)$ for the lift and drag models given in [37] with parameters $M \approx 8.9372$, $\alpha_0 = 0.1426$, $C_{L_0} = 0$, $C_{L_\alpha} = 5.5370$ rad^{-1}, $C_{D_0} = 0.0196$, and $k = 0.0112$.

where $C_{L_0} \in \mathbb{R}$, $C_{L_\alpha} \in \mathbb{R}$ are model parameters and

$$\chi(\alpha) = \frac{1 + e^{-M(\alpha-\alpha_0)} + e^{M(\alpha+\alpha_0)}}{(1 + e^{-M(\alpha-\alpha_0)})(1 + e^{M(\alpha+\alpha_0)})}$$

with $\alpha_0 \in \mathbb{R}$ and $M > 0$. The parameters $M \approx 8.9372$, $\alpha_0 = 0.1426$, $C_{L_0} = 0$, and $C_{L_\alpha} = 5.5370$ rad^{-1} provide a good fit to the airfoil data shown in Fig. 10 as long as $\alpha \in [-0.4, 0.4]$. The parameter $\delta(\alpha)$ for this set of parameters is shown in Fig. 11 and it displays the positive definiteness of $\delta(\alpha)$ for $|\alpha| \leq 0.4$ rad, thus meeting the assumptions on Proposition 4 for a stable transition flight.

We conclude that, depending on the stall behavior, the robustness of the transition controller may be compromised. In an aircraft design phase, thick airfoil profiles are preferred for the envisaged application as they exhibit smoother stall behavior than thin airfoil profiles ([21]).

In Proposition 4 (whose proof is deferred in Appendix A), we verify that the positive definiteness of $\delta(\alpha)$ ensures the stability of the $\tilde{w}$ system. The control authority in the $\tilde{u}$ system is used to keep the influence of perturbations small. Corollary 5 evinces that under the ideal scenario of $\delta(\alpha) > 0$ for all $\alpha \in (-\pi/2, \pi/2)$, the restrictions on the initial error $\tilde{w}(0)$ can be made arbitrarily large as long as we select a high enough controller gain $k_u > 0$ and small enough restrictions on the initial state $\tilde{u}(0)$.

Proposition 4: For any number $\Delta_u > 0$, if $u^\star(t) > 0$ and $\delta(\alpha^\star(t)) > 0$ for all $t \geq 0$, then there exist $c_u > 0$, $c_w > 0$, $\Delta_\theta > 0$, $\Delta_w > 0$, and $k_u^\star > 0$ such that for all $k_u \geq k_u^\star$ the system with the dynamics (15a) and (15b) is rendered ISS with restrictions c_u in the initial state $\tilde{u}(0)$, c_w on the initial state $\tilde{w}(0)$, Δ_u on the input $\delta_u(t)$, Δ_w on the input $\delta_w(t)$ and Δ_θ on the input $(\tilde{q}, \tilde{\theta})$ using the control law defined in (14).

If the aircraft possesses a wing such that $\delta(\alpha) > 0$ for all $\alpha \in (-\pi/2, \pi/2)$, then the system with the dynamics (15a) and (15b) is rendered ISS with arbitrary restrictions on the initial state $\tilde{w}(0)$ as stated in the following corollary, whose proof is deferred in Appendix B.

Corollary 5: For any number $\Delta_u > 0$ and $c_w > 0$, if $u^\star(t) > 0$ for all $t \geq 0$ and $\delta(\alpha) > 0$ for all $\alpha \in (-\pi/2, \pi/2)$, then there exist $c_u > 0$, $\Delta_\theta > 0$, $\Delta_w > 0$, and $k_u^\star > 0$ such that for all $k_u \geq k_u^\star$ the system with the dynamics (15a) and (15b) is rendered ISS with restrictions c_u in the initial state $\tilde{u}(0)$, c_w on the initial state $\tilde{w}(0)$, Δ_u on the input $\delta_u(t)$, Δ_w on the input $\delta_w(t)$, and Δ_θ on the input $(\tilde{q}, \tilde{\theta})$ using the control law defined in (14).

The importance of the result stated in the previous corollary stems from the fact that by establishing c_w arbitrarily improves the system robustness to external disturbances. Due to the shortage of detailed studies on the behavior of airfoils over high angles of attack, it is difficult to assess whether the condition $\delta(\alpha) > 0$ for all $\alpha \in (-\pi/2, \pi/2)$ is satisfied for any other airfoil designs than those presented in [23]. Nevertheless, the data given in [23] and shown in Fig. 10 reveals that there exist in fact airfoils that exhibit this property, albeit marginally, thus suggesting that more sophisticated airfoil designs which delay or smoothen the wing stall might add extra robustness to the proposed control strategy. The following proposition states a rather obvious result, concerning the stability of the system $(\tilde{q}, \tilde{\theta})$.

Proposition 6: For any positive numbers k_q and k_θ, the system with the closed loop of the system dynamics (15c) and (15d) and the control law (14) is ISS without restrictions.

Proof: The unperturbed closed-loop system of the form $\dot{\mathbf{x}} = \mathbf{A}\mathbf{x}$ and it is given by

$$\begin{bmatrix} \dot{\tilde{q}} \\ \dot{\tilde{\theta}} \end{bmatrix} = \begin{bmatrix} -k_\theta k_q & -k_\theta \\ 1 & 0 \end{bmatrix} \begin{bmatrix} \tilde{q} \\ \tilde{\theta} \end{bmatrix} \tag{22}$$

which is a linear-time invariant system and the matrix $\mathbf{A}$ is Hurwitz. It follows then that, for any positive-definite matrix $\mathbf{Q}$, there exists a solution $\mathbf{P}$ to the Lyapunov equation

$$\mathbf{A}^\top \mathbf{P} + \mathbf{P}\mathbf{A} = -\mathbf{Q}$$

such that the function

$$V_2(\mathbf{x}) = \mathbf{x}^\top \mathbf{P} \mathbf{x} \qquad (23)$$

is positive-definite and its derivative

$$\dot{V}_2(\mathbf{x}) = -\mathbf{x}^\top \mathbf{Q} \mathbf{x}$$

is negative-definite, and the unperturbed system is exponentially stable. The perturbed system includes the unknown quantity $\delta_q(t)$, which disturbs the nominal linear system. Adding this perturbation to the linear system (22) provides the following bound on the derivative of the Lyapunov function given in (23):

$$\dot{V}_2 \le -\lambda_{\min}(\mathbf{Q}) \|\mathbf{x}\|^2 + \|\mathbf{x}\| |\delta_q(t)|$$

where $\lambda_{\min}(\mathbf{Q})$ is the eigenvalue of $\mathbf{Q}$ with smallest real part. As a consequence, for any $\eta \in [0, 1)$ it is possible to find that

$$\dot{V}_2 \le -\lambda_{\min}(\mathbf{Q})\eta \|\mathbf{x}\|^2 \quad \|\mathbf{x}\| \ge \frac{|\delta_q(t)|}{(1-\eta)\lambda_{\min}(\mathbf{Q})}. \qquad (24)$$

Thus, the system is ISS without restrictions and with asymptotic gain $1/((1-\eta)\lambda_{\min}(\mathbf{Q}))$. ∎

Not only is the system $(\tilde{q}, \tilde{\theta})$ ISS without restrictions, but it is possible to set $\lambda_{\min}(\mathbf{Q})$ arbitrarily high such that the perturbation influence on the system behavior is arbitrarily small. Employing this insight, the following result proves the stability of the overall system (15).

Proposition 7: For any numbers $\Delta_q > 0$, $\Delta_u > 0$, $k_\theta > 0$, $k_q > 0$, if $u^\star(t) > 0$ and $\delta(\alpha^\star(t)) > 0$ for all $t \ge 0$, then there exist $c_u > 0$, $c_w > 0$, $c_q > 0$, $c_\theta > 0$, $\Delta_q > 0$, $\Delta_w > 0$, and $k_u^\star > 0$ such that for all $k_u > k_u^\star$ the system with the dynamics (15) is rendered ISS with restrictions c_u in the initial state $\tilde{u}(0)$, c_w on the initial state $\tilde{w}(0)$, c_q on the initial state $\tilde{q}(0)$, c_θ on the initial state $\tilde{\theta}(0)$, Δ_u on the input $\delta_u(t)$, Δ_w on the input $\delta_w(t)$, and Δ_q on the input $\delta_q(t)$ using the control law defined in (14).

Proof: Define the set

$$\Omega_2(l) = \{(\tilde{q}, \tilde{\theta}) \in \mathbb{R}^2 : V_2(\tilde{q}, \tilde{\theta}) \le l\}. \qquad (25)$$

For any $c_q > 0$ and $c_\theta > 0$, there exists l_2 such that

$$\{(\tilde{q}, \tilde{\theta}) \in \mathbb{R}^2 : |\tilde{q}| \le c_q \wedge |\tilde{\theta}| \le c_\theta\} \subset \Omega_2(l_2).$$

For any given $\Delta_q > 0$, and using the result in (24), it is possible to set $\lambda_{\min}(\mathbf{Q})$ such that

$$\left\{(\tilde{q}, \tilde{\theta}) \in \mathbb{R}^2 : \|(\tilde{q}, \tilde{\theta})\| < \frac{\Delta_q}{(1-\eta)\lambda_{\min}(\mathbf{Q})}\right\} \subset \Omega_2(l_2).$$

In this situation, the set $\Omega_2(l_2)$ is forward invariant and, if the initial state is within this set, the system state does not leave $\Omega_2(l_2)$ for all time. The result follows from Propositions 4 and 6 as long as the restrictions c_q and c_θ are such that:

$$\Delta_\theta \ge \max_{(\tilde{q}, \tilde{\theta}) \in \Omega_2(l_2)} \|(\tilde{q}, \tilde{\theta})\|$$

employing the relation (25). ∎

The required initial conditions for Proposition 7 are enforced by the switching logic, which only enables the transition controller when $\tilde{q}(0) \le c_q$ and $\tilde{\theta}(0) \le c_\theta$ are satisfied.

In short, this section presented a trajectory tracking controller for the underactuated system described in Section III. This controller is input-to-state stable with restrictions on the disturbances and on the initial tracking errors. Moreover, it relies on the wing lift/drag characteristics which are measured by means of $\delta(\alpha)$ provided in (19).

C. Recovery Controller

The controller developed throughout this section for the aircraft dynamic system (6) achieves almost global stabilization of the hover equilibrium point, characterized by

$$u_{\mathrm{eq}} = 0 \text{ m/s} \quad w_{\mathrm{eq}} = 0 \text{ m/s}$$
$$q_{\mathrm{eq}} = 0 \text{ rad/s} \quad \Theta_{\mathrm{eq}} = 0 \text{ rad}$$

where $\Theta = \theta - \pi/2$ using the Z-X-Y Euler angle parametrization of $\mathbf{R} \in SO$ (3a) and (3b). Moreover, the control law provides $T \ge T_{\min}$ for all $t \ge 0$, under an appropriate choice of parameters.

The longitudinal controller design relies on Lyapunov stability principles and it is obtained through standard backstepping techniques (see [38]). In the next section, the equilibrium point $(\dot{x}, \dot{z}, \Theta - \Theta^\star, q - q^\star) = 0$ is rendered almost globally exponentially stable[1] for the unperturbed system ($\delta_u(t) = \delta_w(t) = \delta_q(t) = 0$ for all $t \ge 0$), and ISS for the perturbed case, given the control law

$$\tau_u = \frac{g}{\cos \Theta^\star}\left(1 + \lambda_z \sigma\left(\frac{k_z \dot{z}}{\lambda_z}\right)\right) \qquad (26a)$$

$$\tau_q = \dot{q}^\star - k_q(q - q^\star) - \frac{\sin(\Theta - \Theta^\star)}{\Gamma_2} \qquad (26b)$$

$$\Theta^\star = \lambda_x \sigma\left(\frac{k_x \dot{x}}{\lambda_x}\right) \qquad (26c)$$

$$q^\star = \Gamma_1 \dot{x} \tau_u \frac{\sin \Theta - \sin \Theta^\star}{\sin(\Theta - \Theta^\star)} + \Gamma_1 \dot{z} \tau_u \frac{\cos \Theta - \cos \Theta^\star}{\sin(\Theta - \Theta^\star)}$$
$$- k_\Theta \frac{\sin(\Theta - \Theta^\star)}{(1 + \cos(\Theta - \Theta^\star))^2} + \dot{\Theta}^\star \qquad (26d)$$

where $\tau_u := T/m$, $\tau_q := M/\mathbf{I}_{yy}$, Γ_1, Γ_2, k_x, k_z, k_Θ, k_q, and λ_x are controller parameters and $\sigma(s)$ denotes the saturation function.

1) Unperturbed System: In this section, we focus on the case where $\delta_u(t) = \delta_w(t) = \delta_q(t) = 0$ for all $t \ge 0$, and prove that (26) renders the equilibrium point $(\dot{x}, \dot{z}, \tilde{\Theta}, \tilde{q}) = 0$, almost globally exponentially stable. In order to improve the clarity of this paper, we present each of the backstepping iterations before the main result.

Consider the aircraft subsystem comprising the dynamics of the states $(\dot{x}, \dot{z})$ and consider the following Lyapunov function candidate $V_1 = \Gamma_1(\dot{x}^2 + \dot{z}^2)/2$, where $\Gamma_1 > 0$ and whose time derivative is given by (provided that $\delta_u(t) = \delta_w(t) = \delta_q(t) = 0$):

$$\dot{V}_1 = \Gamma_1 \dot{x}(\dot{u}\cos\theta - qu\sin\theta + \dot{w}\sin\theta + qw\cos\theta)$$
$$+ \Gamma_1 \dot{z}(-\dot{u}\sin\theta - qu\cos\theta + \dot{w}\cos\theta - qw\sin\theta). \qquad (27)$$

---

[1] See [39] for further details on almost global stability of dynamic systems.

Replacing (6a)–6(e) into (27) yields

$$\dot{V}_1 = -\Gamma_1\tau_u\sin\Theta\dot{x} - \Gamma_1\frac{\rho A}{2m}\|\mathbf{v}\|^{\frac{3}{2}}C_D(\alpha) - \Gamma_1\tau_u\cos\Theta\dot{z} + \Gamma_1 g\dot{z} \tag{28}$$

where we have used the relations $\tau_u := T/m$, $\cos\theta = -\sin\Theta$ and $\sin\theta = \cos\Theta$. Letting $\Theta = \Theta^\star$ and replacing (26a) and (26c) into (28) yields

$$\begin{aligned}\dot{V}_1\big|_{\Theta=\Theta^\star} = &-\Gamma_1\tau_{u_{\min}}\dot{x}\sin\left(\lambda_x\sigma\left(\frac{k_x\dot{x}}{\lambda_x}\right)\right)\\ &-\Gamma_1\frac{\rho A}{2m}\|\mathbf{v}\|^{\frac{3}{2}}C_D(\alpha) - \Gamma_1\dot{z}\sigma\left(\frac{k_z\dot{z}}{\lambda_z}\right)\end{aligned} \tag{29}$$

where $\tau_{u_{\min}} \leq \min_{t\geq 0}\tau_u(t)$. The condition $\tau_{u_{\min}} > 0$ is met, provided that $\lambda_x \in (0, \pi/2)$ and $\lambda_z \in (0, 1)$, as proved in the following lemma.

Lemma 8: Let τ_u and $\Theta^\star$ be defined by (26a) and (26c), respectively, and let $\sigma : \mathbb{R} \to \mathbb{R}$ be the function with the properties described in Section II. For any λ_x, λ_z verifying $\lambda_x \in (0, \pi/2)$ and $\lambda_z \in (0, 1)$, there exist $\tau_{u_{\min}} > 0$ and $\tau_{u_{\max}} > 0$ such that

$$\tau_{u_{\min}} < \tau_u(t) \leq \tau_{u_{\max}} \tag{30}$$

for all $t \geq 0$.

Proof: From the properties of the saturation function we know that $-1 \leq \sigma(s) \leq 1$, therefore we may conclude that

$$-\lambda_x \leq \lambda_x\sigma\left(\frac{k_x\dot{x}}{\lambda_x}\right) \leq \lambda_x \qquad -\lambda_z \leq \lambda_z\sigma\left(\frac{k_z\dot{z}}{\lambda_z}\right) \leq \lambda_z. \tag{31}$$

Replacing (26a) and (26c) in (31), we conclude that $-\lambda_x \leq \Theta^\star \leq \lambda_x$. For $|\lambda_x| < \pi/2$ we have that $\cos(-\lambda_x) = \cos(\lambda_x) > 0$, and the following holds:

$$0 < \frac{g}{\cos(\lambda_x)}(1-\lambda_z) \leq \tau_u \leq \frac{g}{\cos(\lambda_x)}(1+\lambda_z)$$

if and only if $\lambda_z \in (0, 1)$. It is easy to check that $\tau_{u_{\min}} = g(1-\lambda_z)/\cos(\lambda_x) > 0$ and $\tau_{u_{\max}} = g(1+\lambda_z)/\cos(\lambda_x) > 0$ satisfy (30), thus concluding the proof. ∎

Applying the property of the saturation function $\sigma(s)s > 0$ to (29), we conclude that for any $k_x > 0$, $k_z > 0$, $\lambda_x \in (0, \pi/2)$ and $\lambda_z \in (0, 1)$, the relation $\dot{V}_1(\dot{x}, \dot{z})|_{\Theta=\Theta^\star} < 0$ holds for all $(\dot{x}, \dot{z}) \neq 0$, under the mild assumption that $C_D(\alpha) > 0$ for all $\alpha \in (-\pi, \pi]$. Therefore, the closed-loop system resulting from the interconnection between the dynamics (6a) and (6b) with (26a) and (26c) has a globally asymptotically stable equilibrium point at $(\dot{x}, \dot{z}) = 0$. This concludes the first iteration of the backstepping procedure.

For the second backstepping iteration, we extend the dynamic system in order to include the dynamics 6(f). We define the error variable $\tilde{\Theta} := \Theta - \Theta^\star$ and consider the following Lyapunov function candidate $V_2(\dot{x}, \dot{z}, \tilde{\Theta}) = V_1(\dot{x}, \dot{z}) + 1 - \cos(\tilde{\Theta})$, whose time derivative is given by

$$\dot{V}_2 = \dot{V}_1 + \sin(\tilde{\Theta})(q - \dot{\Theta}^\star). \tag{32}$$

Letting $q = q^\star$, and replacing (26d) and (28), into (32) yields

$$\dot{V}_2\big|_{q=q^\star} = -\Gamma_1\tau_u\dot{x}\sin\Theta^\star - \Gamma_1\frac{\rho A}{2m}\|\mathbf{v}\|^{\frac{3}{2}}C_D(\alpha)$$

$$-\Gamma_1\tau_u\dot{z}\cos\Theta^\star - k_\Theta\tan^2\left(\frac{\tilde{\Theta}}{2}\right). \tag{33}$$

Replacing (26) into (33) yields

$$\begin{aligned}\dot{V}_2\big|_{q=q^\star} = &-\Gamma_1\tau_{u_{\min}}\dot{x}\sin\left(\lambda_x\sigma\left(\frac{k_x\dot{x}}{\lambda_x}\right)\right) - \Gamma_1\dot{z}\sigma\left(\frac{k_z\dot{z}}{\lambda_z}\right)\\ &-\Gamma_1\frac{\rho A}{2m}\|\mathbf{v}\|^{3/2}C_D(\alpha) - k_\Theta\tan^2\left(\frac{\tilde{\Theta}}{2}\right)\end{aligned} \tag{34}$$

which verifies $\dot{V}_2|_{q=q^\star} < 0$ for all $(\dot{x}, \dot{z}, \dot{\Theta}) \notin \{0\}\cup\{(0, 0, \pi)\}$. The proposed control law given in (26) is almost globally asymptotically stable in the sense that there is a set of Lebesgue measure zero, given by $\{(0, 0, \pi)\}$, that does not belong to the domain of attraction for the equilibrium point $(\dot{x}, \dot{z}, \dot{\Theta}) = 0$. From the previous iterations of the backstepping procedure, we are able to derive the following proposition which constitutes the main contribution of this paper.

Proposition 9: For any $\Gamma_1 > 0$, $\Gamma_2 > 0$, $k_x > 0$, $k_z > 0$, $k_\Theta > 0$, $k_q > 0$, and $\lambda_x \in (0, \pi/2)$, if $C_D(\alpha) > 0$ for all $\alpha \in (-\pi, \pi]$ and $\delta_u(t) = \delta_w(t) = \delta_q(t) = 0$, then the origin of the closed-loop system resulting from the interconnection between (6) and the control law (26) is almost globally exponentially stable. Moreover, the thrust $T(t)$ is bounded for all $t \geq 0$.

Proof: The boundedness of T follows from Lemma 8. We now resort to the Lyapunov candidate function

$$V(\dot{x}, \dot{z}, \tilde{\Theta}, \tilde{q}) = V_2(\dot{x}, \dot{z}, \tilde{\Theta}) + \frac{\Gamma_2}{2}\tilde{q}^2 \tag{35}$$

where $\tilde{\Theta} := \Theta - \Theta^\star$ and $\tilde{q} := q - q^\star$. This function is positive definite and continuously differentiable in the domain $\mathbb{R}^3 \times (-\pi, \pi)$ and its time derivative is given by

$$\dot{V} = \dot{V}_2 + \Gamma_2\tilde{q}(\tau_q - \dot{q}^\star). \tag{36}$$

Replacing (32) into (36) and using $\tilde{q} := q - q^\star$, we obtain

$$\begin{aligned}\dot{V} &= \dot{V}_1 + \sin(\tilde{\Theta})(\tilde{q} + q^\star - \dot{\Theta}^\star) + \Gamma_2\tilde{q}(\tau_q - \dot{q}^\star)\\ &= \dot{V}_2\big|_{q=q^\star} + \tilde{q}\sin(\tilde{\Theta}) + \Gamma_2\tilde{q}(\tau_q - \dot{q}^\star).\end{aligned} \tag{37}$$

Replacing (34) and (26b) into (37) yields

$$\begin{aligned}\dot{V} = &-\Gamma_1\tau_{u_{\min}}\dot{x}\sin\left(\lambda_x\sigma\left(\frac{k_x\dot{x}}{\lambda_x}\right)\right) - \Gamma_2 k_q\tilde{q}^2\\ &-\Gamma_1\frac{\rho A}{2m}\|\mathbf{v}\|^{3/2}C_D(\alpha) - \Gamma_1\dot{z}\sigma\left(\frac{k_z\dot{z}}{\lambda_z}\right) - k_\Theta\tan^2\left(\frac{\tilde{\Theta}}{2}\right)\end{aligned} \tag{38}$$

where $\tau_{u_{\min}}$ is found from the results in Lemma 8, using the properties $\lambda_x \in (0, \pi/2)$ and $\lambda_z \in (0, 1)$. The Lyapunov function time derivative provided in (38) alone justifies almost global asymptotic stability employing standard Lyapunov arguments. In order to prove the almost global exponential stability of $(\dot{x}, \dot{z}, \tilde{\Theta}, \tilde{q}) = 0$, two steps are required: 1) notice that near $(\dot{x}, \dot{z}) = (0, 0)$ the effect of the saturated control inputs has primacy over that of the aerodynamic drag and 2) verify that far from the origin, the drag contribution supersedes the control inputs, providing almost global exponential stability.

Let us define the set-valued map $\Omega(\ell) : \mathbb{R} \rightrightarrows \mathbb{R}^2$ as $\Omega(\ell) = \{(\dot{x}, \dot{z}) \in \mathbb{R}^2 : \|(\dot{x}, \dot{z})\| \leq \ell\}$. Due to the properties

of the saturation function highlighted in Section II, for every $\overline{\ell} > 0$ it is possible to find $L_\sigma > 0$ such that $L_\sigma k_z \dot{z}^2 \leq \dot{z} \lambda_z \sigma(k_z \dot{z}/\lambda_z)$, $L_\sigma (2/\pi) k_x \dot{x}^2 \leq \dot{x} \sin(\lambda_x \sigma(k_x \dot{x}/\lambda_x))$, hold true for all $(u, w) \in \Omega(\overline{\ell})$, because $s \sin(s) \geq 2s^2/\pi$, for all $s \in [-\pi/2, \pi/2]$ (and $\lambda_x \in (0, \pi/2)$).

Using the relation $\tan^2(\Theta/2) \geq \Theta^2/4 \geq (1 - \cos(\Theta))/4$, for all $\Theta \in (-\pi, \pi)$, the Lyapunov function time derivative has the following upper bound in $\Omega(\overline{\ell}) \times \mathbb{R} \times (-\pi, \pi)$:

$$\dot{V} \leq -\Gamma_1 \tau_{u_{\min}} L_\sigma k_z \dot{z}^2 - \Gamma_1 \frac{2}{\pi} g L_\sigma k_x \dot{x}^2$$
$$- \Gamma_2 k_q \tilde{q}^2 - \frac{k_\theta}{4}(1 - \cos \widetilde{\Theta}).$$

Since $C_D(\alpha) > 0$ it is possible to find $C_{D_0} \in \mathbb{R}$ such that $C_{D_0} = \min_{\alpha \in (-\pi, \pi]} C_D(\alpha)$. Moreover, selecting $\underline{\ell}$ such that $0 < \underline{\ell} < \overline{\ell}$ provides the following bound on the Lyapunov function derivative:

$$\dot{V} \leq -\frac{\Gamma_1 \rho A \underline{\ell} C_{D_0}}{2m}(\dot{x}^2 + \dot{z}^2) - \Gamma_2 k_q \tilde{q}^2 - \frac{k_\theta}{4}(1 - \cos \widetilde{\Theta})$$

for all $(\dot{x}, \dot{z}, \widetilde{\Theta}, \tilde{q}) \in \Omega(\underline{\ell}) \times \mathbb{R} \times (-\pi, \pi)$. Defining

$$\Gamma = \min\{2\tau_{u_{\min}} L_\sigma k_z, 4g L_\sigma k_x/\pi$$
$$(\rho A \underline{\ell} C_{D_0})/m, 2k_q, k_\theta/4\}$$

which verifies $\Gamma > 0$, the following holds:

$$\dot{V} \leq -\Gamma V \qquad (39)$$

for all $(\dot{x}, \dot{z}, \widetilde{\Theta}, \tilde{q}) \in \mathbb{R}^3 \times (-\pi, \pi)$. It follows from standard Lyapunov arguments that the origin is almost globally exponentially stable. ∎

Analyzing (38) we notice two different contributions to the aircraft stability: 1) the aerodynamic drag, embodied by the $C_D(\alpha)$ term; and 2) the saturated control inputs, embodied by the saturated actuations on the aircraft velocity: $\lambda_x \sigma(k_x \dot{x}/\lambda_x)$ and $\lambda_z \sigma(k_z \dot{z}/\lambda_z)$. Neither of these contributions taken alone suffices to prove almost global exponential stability of the origin but, combining the two contributions together, the aforementioned property is verified. A remarkable feature of the proposed controller is that its performance does not depend on the coefficient of lift evolution with the angle of attack, and so, wing stall and other related subtleties are rendered meaningless in this application. It should be noted that throughout the design of the recovery controller we assume that: 1) the aircraft movement is constrained to the vertical plane, and 2) the elevator has full control authority. We rely on active lateral regulation to overcome deviations from the vertical plane and, when the velocity is close to zero, the elevator is guaranteed to have some degree of control authority because of the propeller's slipstream. However, this actuation is certainly not unbounded and the controller might fail if the conditions are too adverse. In the next section, the behavior of the aircraft system is analyzed in the presence of unknown perturbations. The almost global exponential stability of the unperturbed system demonstrated in Proposition 9 plays a key role when studying the effects of these perturbations.
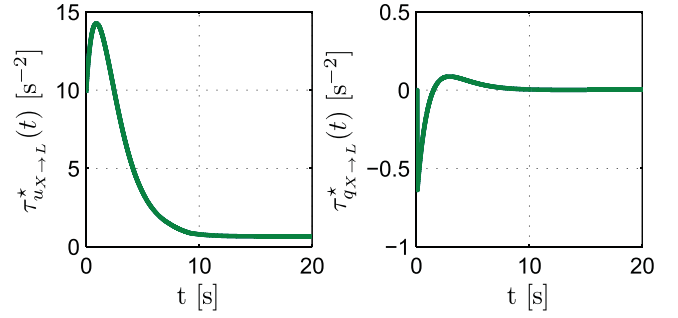

Fig. 12. Reference actuator inputs for the transition maneuver from hover to level. For these maneuvers, we have $\nu_T \approx 0.45$ and $\nu_M = 6.9 \times 10^{-3}$ rad/s^2.

2) Perturbed System: Considering $\delta_u(t)$, $\delta_w(t)$, and $\delta_q(t)$ as inputs, the aircraft system (6), subject to (26), is ISS as stated in Proposition 10.

Proposition 10: The closed-loop system resulting from the interconnection between (6) and (26), satisfying the assumptions of Lemma 8, is ISS with respect to the disturbances $\delta_u(t)$, $\delta_w(t)$, and $\delta_q(t)$ if $C_D(\alpha) > 0$ for all $\alpha \in (-\pi, \pi]$.

Proof: Take (35) to be a Lyapunov function candidate. One must compute its time derivative for the case where the disturbances $\delta = [\delta_u(t), \delta_w(t), \delta_q(t)]^\top$ are nonzero. Recombining (27) and (6) for this situation one finds that

$$\dot{V}_1 \leq \dot{V}_1|_{\delta=0} + 2\|(\dot{x}, \dot{z})\|(|\delta_u(t)| + |\delta_w(t)|) \qquad (40)$$

making use of the relations $|\dot{x}|, |\dot{z}| \leq \|(\dot{x}, \dot{z})\|$, $|\cos(s)| \leq 1$, and $|\sin(s)| < 1$. Using (40) and the relation (39), the derivative of (35) is upper bounded by

$$\dot{V} \leq -\Gamma V + 2\|(\dot{x}, \dot{z}, \widetilde{\Theta}, \tilde{q})\|(|\delta_u(t)| + |\delta_w(t)| + |\delta_q(t)|). \quad (41)$$

Introducing the variable $\zeta \in (0, 1)$ into (41), the following relation is derived:

$$\dot{V} \leq -\Gamma(1 - \zeta)V,$$
$$\text{for } \|(u, w, \tilde{q}, \widetilde{\Theta})\| \geq 2\frac{|\delta_u(t)| + |\delta_w(t)| + |\delta_q(t)|}{\Gamma \zeta}.$$

It follows that, the closed-loop system is input-to-state stable with asymptotic gain $2(\Gamma\zeta)^{-1}$. ∎

D. Lateral Controller

The lateral controller objective is to keep the aircraft motion constrained to the vertical plane. Therefore, the lateral variables (v, p, r, ϕ, ψ) should not deviate too far from the desired values $(v_{\text{eq}}, p_{\text{eq}}, r_{\text{eq}}, \phi_{\text{eq}}, \psi_{\text{eq}}) = 0$. Lateral regulation is provided by means of a state feedback control law $\boldsymbol{\mu}_{\text{lat}} = -\mathbf{K}_q \boldsymbol{\xi}_{\text{lat}}$, where $q \in \mathcal{Q}$, $\boldsymbol{\mu}_{\text{lat}} = [L_a\ N_a]^\top$, $\boldsymbol{\xi}_{\text{lat}} = [v\ p\ r\ \phi\ \psi\ x_1\ x_2]^\top$, $\mathbf{K} \in \mathbb{R}^{2 \times 7}$ is the control gain and x_1, x_2 are suitable integrator states. This strategy robustly stabilizes the aircraft within a sublevel set of the Lyapunov function $V(\boldsymbol{\xi}) = \boldsymbol{\xi}^\top \boldsymbol{\xi}$ near the linearization point $(\boldsymbol{\xi}_0, \boldsymbol{\mu}_0) = 0$ (see [38]).

The selection of the integrator states is dependent on the specific Euler angle parametrization, which was chosen for each operating mode. For the attitude parametrization on the hover and transition operating mode, we chose the Z-Y-X
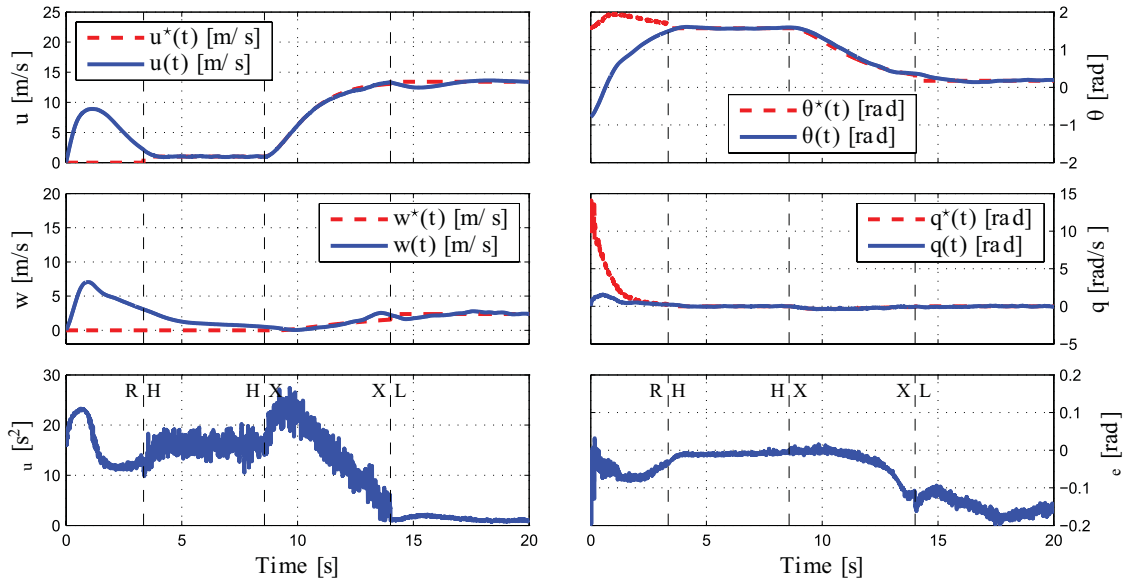
Fig. 13. Simulation results (first run). The aircraft starts in recovery and it is stabilized in hovered flight, the hover controllers provide increased stabilization before switching to the transition operating mode. The aircraft reaches level operating mode as expected.

Euler angle parametrization but, to avoid parametrization singularities, we employed the Up-East-North inertial reference frame. For these two operating modes, the selected integrator states are $x_1 = v$ and $x_2 = \phi$. For the level operating mode, we use also the standard Z-Y-X Euler angles and the NED inertial reference frame. The selected integrator states are $x_1 = v$ and $x_2 = \psi$. For the recovery operating mode, we employ the Z-X-Y Euler angle parametrization and the integrator states $x_1 = v$ and $x_2 = \psi$. This parametrization does not exhibit any singularities for trajectories taking place near the vertical plane. Also, it preserves the well-known decoupling between the lateral and longitudinal dynamics, enabling the lateral controller to be designed separately (see [20]). We employ standard linear optimal techniques on the dimensioning of the controller's gain.

In the next section, we present the simulation results which assess the controller's performance.

VII. SIMULATION

The simulation presented in this section shows the controller's ability to perform the transition from hovered flight to leveled flight regardless of the initial condition. The simulation environment is based on the open-source simulation tool for hybrid systems presented in [40], and the aircraft model was obtained based on the aircraft depicted in Fig. 2.

A. Simulation Data

The selected hover and level equilibrium points are given by

$$u_{H_{eq}} = 0 \text{ m/s} \quad u_{L_{eq}} \approx 13.4 \text{ m/s}$$
$$w_{H_{eq}} = 0 \text{ m/s} \quad w_{L_{eq}} \approx 2.4 \text{ m/s}$$
$$q_{H_{eq}} = 0 \text{ rad/s} \quad q_{L_{eq}} = 0 \text{ rad/s}$$
$$\theta_{H_{eq}} = 90° \quad \theta_{L_{eq}} \approx 10°$$

respectively. The hover and level controllers locally stabilize the given equilibrium points and are designed according to the

strategy defined in Section VI-A with $\tilde{u}_{q_{max}} = -\tilde{u}_{q_{min}} = 1$ m/s and $\tilde{\theta}_{q_{max}} = -\tilde{\theta}_{q_{min}} = 5°$.

The transition controller parameters are $k_\theta = 10$ 1/s^2, $k_u = 10$ s^{-1}, and $k_q = 1$ 1/s. The recovery controller parameters are $\Gamma_1 = 0.001$, $\Gamma_2 = 30$, $k_\Theta = 0.1$ s^{-1}, $k_q = 2$ s^{-1}, $k_u = 1$ s^{-1}, $k_w = 0.1$ s^{-1}, $\lambda_u = 0.5$, $\lambda_w = \pi/4$, and $\epsilon = 2$.

The remaining aircraft parameters are $m = 1.64$ kg, $\mathbf{I}_{yy} = 0.08$ kg.m^2, $A_w = 0.29$ m^2, $b = 1.07$ m, $\rho = 1.225$ kg/m^3, $g = 9.81$ m/s^2, $x_{ac_{hs}} = -0.56$ m, $A_{hs} = 0.0575$ m^2, $A_p = 0.0415$ m^2, and $A_{p,hs} = 0.0155$ m^2. Moreover, the chosen airfoil is the NACA0025 whose lift and drag profiles are depicted in Fig. 10.

For the simulations presented in this section, the state measurements used for feedback are corrupted with additive zero-mean white noise, simulating sensor noise. The standard deviation of aircraft velocity measurement errors is 0.1 m/s and the attitude of the vehicle, in roll, pitch, and yaw Euler angles, is corrupted by noises with standard deviation of 0.1° for the roll, pitch, and yaw. Finally, the angular velocity measurements are corrupted with a 0.05°/s standard deviation noise.

B. Reference Trajectory

As the reference trajectory, we employ the maneuver described in Section V and depicted in Fig. 7. It is possible to check that $u^\star(t) > 0$ and $\delta(\alpha^\star(t)) > 0$ for the proposed trajectories, otherwise, the results stated in Proposition 4 would not be verified. The reference inputs $\tau^\star_{q_{X \to L}}(t)$ and $\tau^\star_{u_{X \to L}}(t)$ resulting from the inversion of the nominal system are depicted in Fig. 12.

C. Simulation Results

The simulation's initial conditions for the first simulation run are

$$u_0 = 0 \text{ m/s} \quad w_0 = 0 \text{ m/s},$$
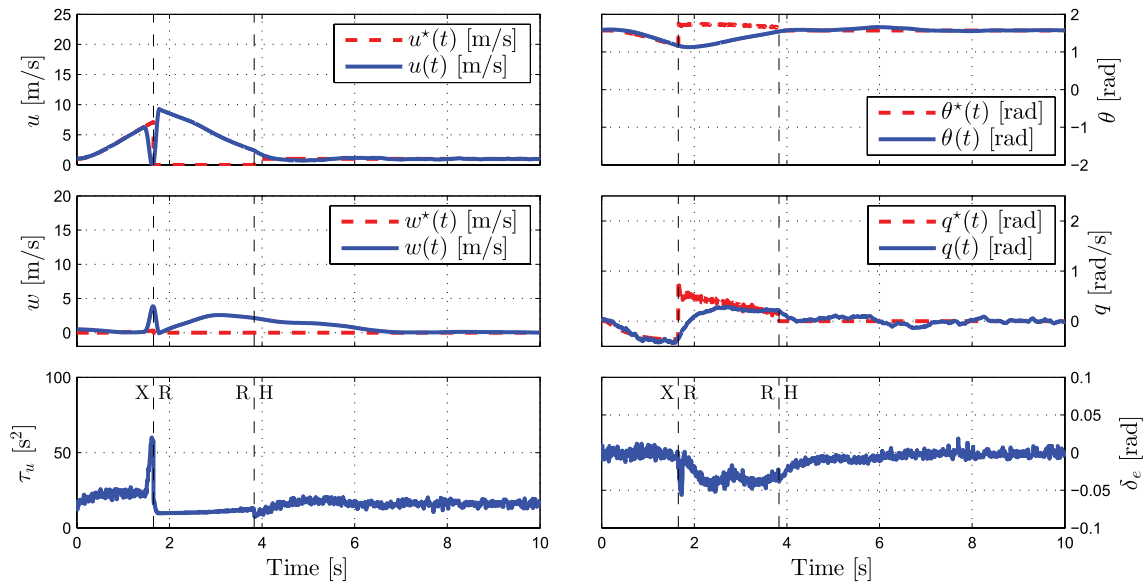$$q_0 = 0 \text{ rad} \quad \theta_0 = -\frac{3\pi}{4} \text{ rad}.$$

Fig. 14.   Simulation results (second run). The aircraft attempts a transition maneuver. The transition is not fully performed due to unexpected disturbances and the recovery mode is entered in order to retry the transition once again.

Under normal operation, the controller should:

1) stabilize the aircraft in hovered flight;
2) switch from recovery to hover, fine-tuning hovered flight stabilization;
3) begin transition reference tracking;
4) switch to the level controller.

Fig. 13 depicts the first simulation run results where the aircraft operated as expected, recovering from awkward initial conditions and performing successfully the transition maneuver, even in the presence of sensor noise and deviations from the vertical plane. It is possible to notice that these disturbances affect the downward velocity w the most because this direction does not have a direct control input. Also, notice that the starting condition is highly unfavorable for stabilization in hovered flight and that aircraft deployment should not be performed with the aircraft facing down unless there is enough ground clearance, because for such initial conditions the aircraft will accelerate toward the ground. Again, the larger the aircraft scale, the larger the ground clearance.

Second, we study a situation where the aircraft is not be able to complete the transition in the presence of a severe wing gust. The recovery mode provides the possibility to retry the transition maneuver, as depicted in Fig. 14. In this simulation run, during the transition, we inflict a wind gust along the negative z-axis of the inertial reference frame with the one-cosine profile [41], a magnitude of 10 m/s, and a duration of 1 m (see Fig. 15), driving the aircraft state to undesirable values. The recovery controller is then activated, taking the aircraft to the hover operating mode so that it may retry the transition maneuver.

Although the lateral variables are not depicted in Figs. 13 and 14, they remain bounded within reasonable values for the simulations we performed.
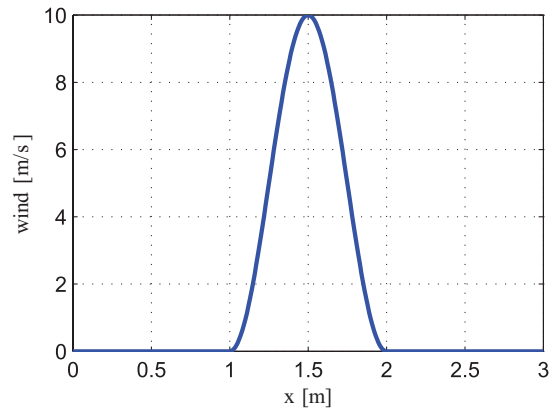

Fig. 15.   One-cosine wind gust profile.

VIII. CONCLUSION

Throughout this paper, a novel hybrid control methodology for a fixed-wing VTOL aircraft was developed. The proposed controller relies on the Hybrid Automaton framework, dividing the flight envelope into four different regions: hover, transition, level, and recovery. The proposed controller employed linear optimal control techniques while in hover or level, providing local stabilization for trajectories in a polytopic region of the flight envelope. A nonlinear controller that renders the closed-loop dynamics input-to-state stable was developed for practical reference tracking. The airfoil characteristics, reference constraints, and controller restrictions, which enable this property, were discussed and a single parameter which characterizes the inherent stability of the system was introduced. The nonlinear controller designed for the recovery operating mode almost globally exponentially stabilizes the hover equilibrium point, allowing for this point to be reached from any flight condition. Simulation results, performed with the full nonlinear model for the aircraft, assessed the controller's performance and robustness.

There are three major open questions arising from this paper that should be addressed in the future. The first one concerns the region of attraction of the lateral controller throughout the recovery maneuver. Although we have shown by simulation that lateral stabilization is achieved by designing a lateral controller separately from the longitudinal controller, it is still not clear whether this strategy works for all the flight conditions spanned throughout the recovery maneuver. Future work on this subject includes the design of a recovery controller which does not rely on the separation between lateral and longitudinal controllers. The second main issue to be addressed in future work is the input saturation. Throughout this paper, it was assumed that there exist controller parameters which enable the inputs to remain bounded. Although this assumption is fine for the local controllers, it might not be true for the recovery controller. If we consider input saturation, we should replace the notion of almost global stabilization by the concept of semi-global stabilization and try to determine, which are the maximum perturbations that the controller is able to overcome. Finally, it is important to improve the robustness of the controller to aerodynamic stall.

APPENDIX

A. Proof of Proposition 4

Consider the Lyapunov function

$$V_1(\tilde{u}, \tilde{w}) = \frac{1}{2}\left(\frac{\tilde{u}^2}{r_u^2} + \frac{\tilde{w}^2}{r_w^2}\right) \qquad (42)$$

and the level set definition given by

$$\Omega_1(l) = \{(\tilde{u}, \tilde{w}) \in \mathbb{R}^2 : V_1(\tilde{u}, \tilde{w}) \le l\}. \qquad (43)$$

It turns out that, due to radial unboundedness, for any $r_u \in \mathbb{R}$ and $r_w \in \mathbb{R}$ there exists positive l_1 such that

$$\{(\tilde{u}, \tilde{w}) \in \mathbb{R}^2 : |\tilde{u}| \le c_u \wedge |\tilde{w}| \le c_w\} \subset \Omega_1(l_1). \qquad (44)$$

In order to show that the closed-loop system has the ISS with restrictions property, we show that the level set $\Omega_1(l_1)$, containing the initial state, is forward invariant under some restrictions.

The functions defined in (16) are locally Lipschitz since the functions h_u, h_w and h_q are continuous and proper. Therefore, there exist positive L_u and L_w such that for all $(\tilde{u}, \tilde{w}) \in \Omega_1(l_1)$ and $\|(\tilde{q}(t), \tilde{\theta}(t))\|_\infty \le \Delta_\theta$

$$\left\|\Psi_u\left(\tilde{u}, \tilde{w}, \tilde{q}, \tilde{\theta}, t\right)\right\| \le L_u\|(\tilde{u}, \tilde{w}, \tilde{q}, \tilde{\theta})\| \qquad (45)$$

$$\left\|\Psi_w\left(\tilde{u}, \tilde{w}, \tilde{q}, \tilde{\theta}, t\right)\right\| \le L_w\|(\tilde{u}, \tilde{w}, \tilde{q}, \tilde{\theta})\| \qquad (46)$$

holds uniformly for all $t \ge 0$. In particular, for $r_u = r_w = 1$, the Lyapunov function derivative $\dot{V}_1$ is given by

$$\dot{V}_1 = \tilde{u}\left(-k_u\tilde{u} + \Psi_u\left(\tilde{u}, \tilde{w}, \tilde{q}, \tilde{\theta}, t\right) + \delta_u(t)\right)$$
$$+ \tilde{w}\left(\Psi_w\left(\tilde{u}, \tilde{w}, \tilde{q}, \tilde{\theta}, t\right) + \delta_w(t)\right). \qquad (47)$$

Substituting (17) into (47) yields

$$\dot{V}_1 = \tilde{u}\left(-k_u\tilde{u} + \Psi_u\left(\tilde{u}, \tilde{w}, \theta_2 - \frac{\theta_1}{k_q}, \theta_1, t\right) + \delta_u(t)\right)$$
$$+ \tilde{w}\left(\Psi_w|_{\tilde{w}=0} + \left.\frac{\partial \Psi_w}{\partial \tilde{w}}\right|_{\tilde{w}=\tilde{w}_0}\tilde{w} + \delta_w(t)\right).$$

Since $\delta(\alpha^\star(t))$ and $u^\star(t)$ are positive for all $t \ge 0$, there exists a neighborhood $\mathscr{B} \in \mathbb{R}^2$ around the reference trajectory such that

$$\frac{\partial \Psi_w}{\partial \tilde{w}} < 0$$

for all $t \ge 0$. Choosing the restrictions on the initial state such that $\Omega_1(l_1) \subset \mathscr{B}$, it follows that it is possible to find

$$\underline{\Psi}_w = \min_{\substack{t \ge 0 \\ (\tilde{u}, \tilde{w}) \in \Omega_1(l_1)}} \left. -\frac{\partial \Psi_w}{\partial \tilde{w}}\right|_{\tilde{w}=0} \qquad (48)$$

because $\Omega_1(l_1) \subset \mathbb{R}^2$ is compact and Ψ_w is continuously differentiable. Substituting (45), (46), and (48) into (47), the following relation is derived:

$$\dot{V}_1|_{\Omega_1(l_1)} \le -(k_u - L_u)\tilde{u}^2 + |\tilde{u}|(L_u + L_w)|\tilde{w}| - \underline{\Psi}_w\tilde{w}^2$$
$$+ |\tilde{u}|L_u\|(\tilde{q}, \tilde{\theta})\| + |\tilde{u}||\delta_u(t)|$$
$$+ |\tilde{w}|L_w\|(\tilde{q}, \tilde{\theta})\| + |\tilde{w}||\delta_w(t)|. \qquad (49)$$

Employing Young's inequality, it follows that:

$$|\tilde{u}\tilde{w}| \le \frac{1}{2}\left(\zeta\tilde{w}^2 + \frac{1}{\zeta}\tilde{u}^2\right)$$

for any $\zeta > 0$. Substituting the previous relation into (49) yields

$$\dot{V}_1|_{\Omega_1(l_1)} \le -\left(k_u - L_u - \frac{L_u + L_w}{2\zeta}\right)\tilde{u}^2$$
$$+ |\tilde{u}|L_u\|(\tilde{q}, \tilde{\theta})\| + |\tilde{u}||\delta_u(t)|$$
$$- \left(\underline{\Psi}_w - \frac{\zeta(L_u + L_w)}{2}\right)\tilde{w}^2$$
$$+ |\tilde{w}|L_w\|(\tilde{q}, \tilde{\theta})\| + |\tilde{w}||\delta_w(t)|.$$

Therefore, for any $\Delta_u > 0$ there exist $\Delta_w > 0$, $\Delta_\theta > 0$, $\zeta > 0$, and $k_u^\star(\zeta) > 0$ such that for any $k_u \ge k_u^\star$ the system is ISS with restrictions c_u on the initial state $\tilde{u}(0)$, c_w on the initial state $\tilde{w}(0)$, Δ_θ on the input $(\tilde{q}, \tilde{\theta})$, Δ_u on the input $\delta_u(t)$ and Δ_w on the input $\delta_w(t)$.

B. Proof of Corollary 5

Consider the Lyapunov function defined in (42) and the level set definition (43). The relation (44) holds with

$$l_1 = \frac{1}{2}\left(\frac{c_u^2}{r_u^2} + \frac{c_w^2}{r_w^2}\right)$$

and the boundary of the level set $\Omega_1(l_1) \subset \mathbb{R}^2$ is the ellipse defined by the equation

$$\frac{\tilde{u}^2}{\left(c_u^2 + \frac{r_u^2}{r_w^2}c_w^2\right)} + \frac{\tilde{w}^2}{\left(c_w^2 + \frac{r_w^2}{r_u^2}c_u^2\right)} = 1.$$

Since $u^\star(t) > 0$, then for any $c_w > 0$ it is possible to select r_u, r_w and c_u such that

$$\min_{t \geq 0} u^\star(t) > c_u > 0$$

and none of the points $(-u^\star(t), -w^\star(t))$ belong to the level set $\Omega_1(l_1)$. Under these conditions and knowing that $\delta(\alpha) > 0$ for all $\alpha \in [-\pi/2, \pi/2]$, the relation (18) holds for all $(\tilde{u}, \tilde{w}) \in \Omega_1(l_1)$. The proof now proceeds similarly to that of Proposition 4, leading to the following upper bound on the Lyapunov function derivative:

$$\dot{V}_1\big|_{\Omega_1(l_1)} \leq -\left(\frac{1}{r_u^2}(k_u - L_u) - \frac{L_u r_u^{-2} + L_w r_w^{-2}}{2\zeta}\right)\tilde{u}^2$$
$$+ |\tilde{u}|L_u r_u^{-2}\|(\tilde{q}, \tilde{\theta})\| + |\tilde{u}|r_u^{-2}|\delta_u(t)|$$
$$-\left(r_w^{-2}\underline{\Psi_w} - \frac{\zeta(L_u r_u^{-2} + L_w r_w^{-2})}{2}\right)\tilde{w}^2$$
$$+ |\tilde{w}|L_w r_w^{-2}\|(\tilde{q}, \tilde{\theta})\| + |\tilde{w}|r_w^{-2}|\delta_w(t)|.$$

Thus, for any $\Delta_u > 0$ there exists $\zeta > 0$, $k_u^\star(\zeta) > 0$, $\Delta_w > 0$, and $\Delta_\theta > 0$ such that for all $k_u \geq k_u^\star$, the closed-loop system is rendered ISS with restrictions c_u in the initial state $\tilde{u}(0)$, c_w on the initial state $\tilde{w}(0)$, Δ_u on the input $\delta_u(t)$, Δ_w on the input $\delta_w(t)$ and Δ_θ on the input $(\tilde{q}, \tilde{\theta})$.

ACKNOWLEDGMENT

REFERENCES

[1] *The U.S. Air Force Remotely Piloted Aircraft and Unmanned Aerial Vehicle Strategic Vision* US Air Force, New York, 2005.

[2] K. Nonami, "Prospect and recent research & development for civil use autonomous unmanned aircraft as UAV and MAV," *J. Syst. Design Dynamics*, vol. 1, no. 2, pp. 120–128, 2007.

[3] D. Mix, J. Koenig, K. Linda, O. Cifdaloz, V. Wells, and A. Rodriguez, "Toward gain-scheduled h-infinity control design for a tilt-wing aircraft," in *Proc. 43rd IEEE Conf. Decision Control*, vol. 2. Dec. 2004, pp. 1222–1227.

[4] S. Yanguo and W. Huanjin, "Design of flight control system for a small unmanned tilt rotor aircraft," *Chin. J. Aeronaut.*, vol. 22, no. 3, pp. 250–256, 2009.

[5] J. Pflimlin, T. Hamel, P. Soueres, and R. Mahony, "A hierarchical control strategy for the autonomous navigation of a ducted fan flying robot," in *Proc. Int. Conf. Robot. Autom.*, 2006, pp. 1–8.

[6] R. Naldi and L. Marconi, "On robust transition maneuvers for a class of tail-sitter vehicles," in *Proc. Conf. Decision Control*, 2010, pp. 358–363.

[7] L. Marconi and R. Naldi, "Robust full degree-of-freedom tracking control of a helicopter," *Automatica*, vol. 43, no. 11, pp. 1909–1920, 2007.

[8] P. Doherty and P. Rudol, "A UAV search and rescue scenario with human body detection and geolocalization," in *Proc. 20th Australian Joint Conf. Adv. Artif. Intell.*, 2007, pp. 1–13.

[9] D. Casbeer, R. Beard, T. McLain, S.-M. Li, and R. Mehra, "Forest fire monitoring with multiple small UAVs," in *Proc. Amer. Control Conf.*, 2005, pp. 3530–3535.

[10] P. Doherty, G. Granlund, K. Kuchcinski, E. Sandewall, K. Nordberg, E. Skarman, and J. Wiklund, "The witas unmanned aerial vehicle project," in *Proc. 14th Eur. Conf. Artif. Intell.*, 2000, pp. 1–9.

[11] W. E. Green and P. Y. Oh, "A MAV that flies like an airplane and hovers like a helicopter," in *Proc. IEEE/ASME*, Dec. 2005, pp. 1–7.

[12] A. L. Desbiens, A. Asbeck, and M. Cutkosky, "Hybrid aerial and scansorial robotics," in *Proc. IEEE Conf. Robot. Autom.*, Mar. 2010, pp. 1–6.

[13] F. Adrian, J. S. McGrew, M. Valenti, D. Levine, and J. P. How, "Hover, transition, and level flight control design for a single-propeller indoor airplane," in *Proc. AIAA Guidance, Navigat. Control Conf.*, 2007, pp. 1–43.

[14] S. R. Osborne, "Transitions between hover and level flight for a tailsitter UAV," M.S. thesis, Dept. Comput. Sci., Brigham Young Univ., Provo, UT, 2007.

[15] L. Marconi, R. Naldi, and L. Gentili, "A control framework for robust practical tracking of hybrid automata," in *Proc. Joint 48th IEEE Conf. Decision Control*, Dec. 2009, pp. 661–666.

[16] D. Cabecinhas, C. Silvestre, P. Rosa, and R. Cunha, "Path following control for coordinated turn," in *Proc. AIAA Guidance Control Conf.*, 2007, pp. 1–9.

[17] P. Casau, D. Cabecinhas, and C. Silvestre, "Autonomous transition flight for a vertical take-off and landing aircraft," in *Proc. IEEE Conf. Decision Control*, Dec. 2011, pp. 3974–3979.

[18] P. Casau, D. Cabecinhas, and C. Silvestre, "Almost global stabilization of a vertical take-off and landing aircraft in hovered flight," in *Proc. Amer. Control Conf.*, 2012, pp. 1–9.

[19] A. Isidori, L. Marconi, and A. Serrani, *Robust Autonomous Guidance*. New York: Springer-Verlag, 2003.

[20] B. Etkin and L. D. Reid, *Dynamics of Flight—Stability and Control*. New York: Wiley, 1996.

[21] J. D. Anderson, *Fundamentals of Aerodynamics*. New York: McGraw-Hill, 1991.

[22] R. V. Mises, *Theory of Flight*. Toronto, ON, Canada: General Publishing, 1959.

[23] R. E. Sheldahl and P. C. Klimas, "Aerodynamic characteristics of seven symmetrical airfoil sections through 180-degree angle of attack for use in aerodynamic analysis of vertical axis wind turbines," Sandia Nat. Labs., Albuquerque, NM, Tech. Rep. SAND80-2114, 1981.

[24] M.-D. Hua, T. Hamel, P. Morin, and C. Samson, "A control approach for thrust-propelled underactuated vehicles and its application to VTOL drones," *IEEE Trans. Autom. Control*, vol. 54, no. 8, pp. 1837–1853, Aug. 2009.

[25] R. Goebel, R. G. Sanfelice, and A. R. Teel, "Hybrid dynamical systems," *IEEE Control Syst. Mag.*, vol. 29, no. 2, pp. 28–93, Apr. 2009.

[26] L. Marconi, R. Naldi, and L. Gentili, "Modelling and control of a flying robot interacting with the environment," *Automatica*, vol. 47, no. 12, pp. 2571–2583, 2011.

[27] J. P. LaSalle, "An invariance principle in the theory of stability," Center Dynam. Systs. Brown Univ., Providence, RI, Tech. Rep. 66-1, Apr. 1966.

[28] R. H. Stone and G. Clarke, "Optimization of transition maneuvers for a tail-sitter unmanned air vehicle (UAV)," in *Proc. Australian Int. Aerosp. Congr.*, 2001, pp. 1–14.

[29] R. H. Stone, "Configuration design of a canard configured tail-sitter unmanned vehicle using multidisciplinary optimisation," Ph.D. dissertation, Dept. Elect. Eng., Univ. Sydney, Sydney, Australia, 1999.

[30] R. Naldi and L. Marconi, "Optimal transition maneuvers for a class of V/STOL aircraft," *Automatica*, vol. 47, no. 5, pp. 870–879, 2011.

[31] J. Löfberg, "YALMIP: A toolbox for modeling and optimization in MATLAB," in *Proc. CACSD Conf.*, Taipei, Taiwan, 2004, pp. 284–289.

[32] D. Cabecinhas, C. Silvestre, P. Rosa, and R. Cunha, "Path-following control for coordinated turn aircraft maneuvers," in *Proc. AIAA Guidance Navigat. Control Conf. Exhibit*, Aug. 2007, pp. 1–19.

[33] P. Rosa, C. Silvestre, D. Cabecinhas, and R. Cunha, "Autolanding controller for a fixed wing unmanned air vehicle," in *Proc. AIAA Guidance Navigat. Control Conf. Exhibit*, Aug. 2007, pp. 1–8.

[34] S. Boyd, L. El Ghaoui, E. Feron, and V. Balakrishnan, *Linear Matrix Inequalities in System and Control Theory* (Studies App. Math.), vol. 15. Philadelphia, PA: SIAM, Jun. 1994.

[35] G. F. Franklin, J. D. Powell, and A. Emami-Naeini, *Feedback Control of Dynamic Systems*. Reading, MA: Addison-Wesley, 1994.

[36] T. M. Apostol, *Calculus*, vol. 1, 2nd ed. New York: Wiley, 1967.

[37] R. W. Beard and T. W. McLain, *Small Unmanned Aircraft: Theory and Practice*. Princeton, NJ: Princeton Univ. Press, 2012.

[38] H. K. Khalil, *Nonlinear Systems*. Englewood Cliffs, NJ: Prentice-Hall, 2002.

[39] J. Vasconcelos, R. Cunha, C. Silvestre, and P. Oliveira, "Landmark based nonlinear observer for rigid body attitude and position estimation," in *Proc. 46th IEEE Conf. Decision Control*, Dec. 2007, pp. 1033–1038.

[40] R. G. Sanfelice and A. R. Teel, "Dynamical properties of hybrid systems simulators," *Automatica*, vol. 46, no. 2, pp. 239–248, 2009.

[41] *Flying Qualities of Piloted Airplanes*, Standard MIL-F-8785C, 1980.

Pedro Casau received the B.Sc. degree in aerospace engineering and M.Sc. in degree in aerospace engineering from the Instituto Superior Técnico (IST), Lisbon, Portugal, in 2008 and 2010, respectively, where he is currently pursuing the Ph.D. degree in electrical and computer engineering.

He was a member of the Attitude Control Subsystem for the ESEO satellite, working on the design of its control architecture, from 2007 to 2009. His current research interests include nonlinear control, hybrid control systems, vision-based control systems, and controller design for autonomous air-vehicles.

David Cabecinhas received the Licenciatura degree in electrical and computer engineering from the Instituto Superior Técnico (IST), Lisbon, Portugal, in 2006, where he is currently pursuing the Ph.D. degree with the Laboratory for Systems and Robotics in Engineering and Science.

He was a Monitor with the Department of Electrical and Computer Engineering, IST, from 2005 to 2006. His current research interests include guidance, navigation, and control of autonomous vehicles, nonlinear control, vision-based control, and integration of vision and inertial sensors for attitude and position estimation.

Carlos Silvestre (M'07) received the Licenciatura degree, M.Sc. degrees in electrical engineering, and Ph.D. degree in control science from the Instituto Superior Técnico (IST), Lisbon, Portugal, in 1987, 1991, and 2000, respectively.

He has been with the Department of Electrical and Computer Engineering, IST, since 1990, where he is currently an Associate Professor of systems, decision, and control. Since 2012, he has been on leave from IST, and is with the Department of Electrical and Computer Engineering, Faculty of Science and Technology, University of Macau, Macao, China, where he is an Associate Professor. He is involved in research on the subjects of navigation guidance, and the control of air and underwater robots. His current research interests include linear and nonlinear control theory, coordinated control of multiple vehicles, gain-scheduled control, integrated design of guidance and control systems, inertial navigation systems, and mission control and real-time architectures for complex autonomous systems with applications to unmanned air and underwater vehicles.